EXPERIMENTAL STUDY OF REPAIRED CONCRETE VIA EPOXY

A Dissertation
Presented to
The Academic Faculty

by

Rebecca Lauren Tien

In Partial Fulfillment
of the Requirements for the Degree
Master of Science in Civil Engineering

Georgia Institute of Technology
February 2019

EXPERIMENTAL STUDY OF REPAIRED CONCRETE VIA EPOXY

Approved by:

Dr. Lauren Stewart, Advisor
School of Civil Engineering
Georgia Institute of Technology

Dr. Chloé Arson
School of Civil Engineering
Georgia Institute of Technology

Dr. Laurence Jacobs
School of Civil Engineering
Georgia Institute of Technology

Date Approved: [February 27, 2019]

ACKNOWLEDGEMENTS

I would like to first thank my professors at the Georgia Institute of Technology; you have helped me grow into a more educated and experienced engineerer during my graduate studies. I also want to especially thank Dr. Lauren Stewart and Dr. Chloé Arson who spearheaded my committee and project group. Your advice and guidance throughout my time has been immensely gratifying.

In regards to the research I performed, I want to thank everyone who was a part of the project team and lent their support and help. In particular, I want to provide a special thanks to the following who made this thesis possible:

Dr. Nan Gao – for all your immense help in the laboratory and teaching me how to be a better researcher as well as the incredible help with my thesis

Pei Wang and Koochul Ji – for supporting my work and helping my understanding of advanced computer modeling of concrete.

Michael Waters and Jeremy Mitchell – for the amazing help and work you provided me in the lab to complete this research

I also want to thank the members of Stewart Research Group who were there for me during my thesis writing period. I thank you for your support.

In addition, I have a special thank you for the incredible and above and beyond work that Dr. Lauren Stewart and Dr. Nan Gao provided in helping me write and finish this thesis. I am beyond thankful for the help and support you both provided.

But most of all, I would not have been able to complete this work without the love and help from my parents, John and Tracy, my sister, Amanda, and my cat, Ashoka, who kept me on task. Thank you. This thesis is dedicated to all of them.

TABLE OF CONTENTS

LIST OF TABLES

LIST OF FIGURES

LIST OF SYMBOLS AND ABBREVIATIONS

ACI	American Concrete Institute
ASTM	American Society for Testing and Materials
ASR	Alkali Silica Reaction
CH	Calcium Hydroxide
CHP	Cumene Hydroperoxide
COV	Coefficient of Variation
CT	Computer Tomography
DEM	Discrete Element Method
DIC	Digital Image Correlation
DSID	Continuum damage mechanics method
ERDC	US Army Corps of Engineers' Research and Development Center
f'c	Compressive Strength of Concrete
FCM	Fictitious Crack Model
FRP	Fiber Reinforced Polymer
Fps	Frames per second
GDOT	Georgia Department of Transportation
HMWM	High Molecular Weight Methacrylate
ITZ	Interfacial Transition Zone
LVDT	lateral variable differential transmitter
NCHRP	National Cooperative Highway Research Program
PCI	Precast/Prestressed Concrete Institute
XFEM	Extended Finite Element Method

SUMMARY

During pre-stress transfer, the bottom portion of steel-reinforced concrete girders is subjected to an important compression induced by the relaxation of tension in the bars, which opens longitudinal cracks along the horizontal axis. Reactions at the supports induce shear stress, which sometimes translates into additional diagonal cracks at the ends of the girders. During the subsequent lifespan of the girder, a variety of crack patterns can occur, including longitudinal (along the beam axis), transverse (perpendicular to the beam axis), and diagonal cracks.

At present, there is a need to assess the mechanical integrity and sustainability of pre-stressed concrete beams during the entire life cycle of the built infrastructure, which includes crack propagation, crack reparation, and repaired crack aging with possible re-opening. As such, a Georgia Institute of Technology research program, sponsored by the Georgia Department of Transportation, seeks to develop modeling strategies to predict the behavior of cracked concrete repaired by epoxy. In order to develop such strategies, experimental investigations are needed to provide calibration and validation data. This thesis describes the experimental characterization and analysis at both the materials and system level. Three main sets of experiments were conducted: (1) concrete and epoxy-repaired concrete cylinders, (2) mortar cylinders, and (3) concrete beams.

The concrete and epoxy-repaired cylinder experiments consisted of both uniaxial and splitting tension tests and involved a newly developed protocol for including epoxy-repair into these material characterization tests. The mortar cylinder experiments also consisted of uniaxial and splitting tension characterization. Additionally, a study as to the effect of specimen size for computational efficiency was conducted.

Both unreinforced and reinforced concrete beams were tested using a three-point bending procedure. In both cases, both “as-built” and epoxy-repaired specimens were tested for comparison and for model validation. The epoxy-repaired reinforced specimens were loaded to induce cracking of various levels, unloaded, repaired with epoxy, and reloaded to failure. In the cases where the cracks were very small (< 0.006 in), the epoxy did not have a significant effect on the ultimate capacity, but the beam behaved in a more brittle fashion. Interestingly, in the experiments where the cracks were larger (> 0.006 in), the beams exhibited a much higher capacity than the “as-built” and the failure mechanism and ductility of the beam was affected.

CHAPTER 1. INTRODUCTION

1.1 Introduction

During pre-stress transfer, the bottom portion of steel-reinforced concrete girders is subjected to an important compression induced by the relaxation of tension in the bars, which opens longitudinal cracks along the horizontal axis. Reactions at the supports induce shear stress, which sometimes leads to the formation of additional diagonal cracks at the ends of the girders. During the subsequent lifespan of the girder, a variety of crack patterns can occur, including longitudinal (along the beam axis), transverse (perpendicular to the beam axis), and diagonal cracks. When these cracks occur, the National Cooperative Highway Research Program (NCHRP) recommends as follows (Tadros et al., 2010): accept the girders if longitudinal cracks are less than 0.012 in. wide; apply cementitious packing materials to cracks between 0.012 in. and 0.025 in. wide; inject epoxy in cracks that are 0.025 in. to 0.050 in. wide; and reject and replace the girder if cracks are wider than 0.05 in. Alternatively, the Precast Concrete Institute (PCI) Guide (2001) identifies three defect categories: those that can be accepted without repair, those that can be repaired, and those that must be rejected (PCI, 2001). The PCI guide has more detailed troubleshooting and repair procedures, depending on the location, orientation, length, and width of the cracks. It specifies a minimum width for epoxy repair beginning at 0.006 inches.

Experimental studies showed that cracked concrete had lower mechanical strength than intact concrete, and that 80% of the lost concrete strength could be recovered by epoxy injection (Issa and Debs, 2007). It has also been shown that epoxy injection can increase the fatigue resistance of cracked mortar, but that the mechanical performance of repaired

concrete decreases as temperature increases (Shin et al., 2011). In general, repaired beams exhibit a more brittle behavior than intact or corroded beams (Okada et al., 1988). Although the model proposed by L. Bardella (Bardella, 2001) properly describes the nonlinear viscoelastic behavior of epoxy resins in the glassy state, no model has ever been proposed to predict the behavior of cracked concrete repaired by epoxy. At present, there is a need to assess the mechanical integrity and sustainability of pre-stressed concrete beams during the entire life cycle of the built infrastructure, which includes crack propagation, crack reparation, and repaired crack aging with possible re-opening.

1.2 Computational Models

1.2.1 XFEM with Cohesive Segments Model

An initial Continuum Damage Mechanics model (the Differential Stress-Induced Damage model, DSID) was developed to predict the propagation of cracks in three directions in concrete, according to net tension and compression criteria (Xu and Arson, 2014; Xu et al., 2017). The model can predict initiation and direction of service damage at the girder bridge deck scale. At the individual girder scale, the deflection of girders with pre-existing vertical cracks was noticeably more significant than simulations of girders without pre-existing damage. The predictions made by the model confirmed that the DSID simulations were emulating behavior observed in the field. While this model type accurately predicted crack initiation, it was unable to predict crack propagation, rather only a general area where a crack was most likely to initiate. As a result, a new researcher investigated an eXtended Finite Element Method (XFEM) with cohesive segments model to simulate discrete crack propagation of concrete (Ji et al., 2019). The model was designed

partially after the Hillerborg Fictitious Crack Model fracture mechanics method (Hillerborg et al., 1976).

While the macro-scale XFEM model simulated fracture propagation in the damaged zone, greater experimental calibration was necessary to more accurately simulate the concrete-epoxy-repaired system using a High Molecular Weight Methacrylate (HMWM) epoxy. As a result, a main objective of this thesis was to provide experimental results to successfully validate -- or, if needed, calibrate -- the XEFM with cohesive segments method.

1.2.2 Discrete Element Method Model

While the XFEM with cohesive segments model aimed to predict the location where the crack propagation begins on a concrete girder, Wang et al. (Wang et al., 2019) developed a second model, the Discrete Element Method (DEM) model, to further characterize crack propagation. The DEM model aims to understand the mechanics of crack initiation and propagation at microscopic scale, and then incorporate epoxy to evaluate its use in repair. Specifically, with calibrated model parameters of the mortar matrix, aggregate, and interfacial phases, the model could then be used to evaluate the effects of an epoxy repair on crack propagation by simulating the contact bond breaks between the different phases of concrete. The model uses the displacement softening curve to determine the contact bond breaks as shown in Figure 1. Furthermore, the DEM model aimed to understand the idealized versus realistic interface effects, the effect of aggregate strength on concrete strength, and the fracture propagation at the cylinder scale.

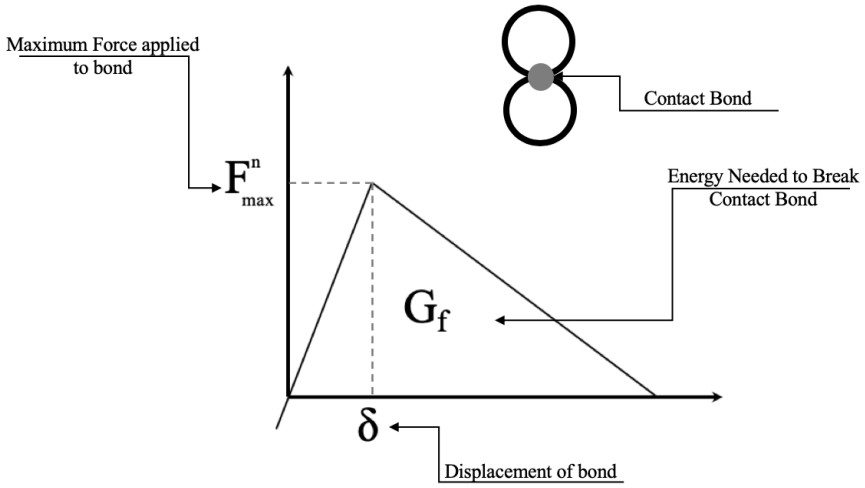

Figure 1: DEM Model Displacement Softening Curve to determine Contact Bond Break (Wang et al., 2019)

Similar to the XFEM with cohesive segments model, the DEM model requires further experimental calibration and validation.

1.3 Research Objectives

Experimental data on the mechanical properties of cracked concrete repaired by epoxy is scarce. The research objective of this thesis was to develop and conduct experiments to measure the mechanical properties of cracked concrete repaired by epoxy in the laboratory, in order to calibrate and validate the computational models created for this research program. The experiments evaluated three specimen types: concrete cylinders, mortar cylinders, and concrete beams. The concrete cylinders were evaluated in both compression and splitting tension and the cylinders were divided into two categories: plain and epoxy repaired. The mortar cylinders were evaluated in compression and splitting tension. The beams consisted of both unreinforced and reinforced specimen and both virgin and epoxy-repaired specimen was experimentally characterized.

1.4 Thesis Organization

Chapter 2 of this thesis consistents of the literature review conducted on fracture mechanic and crack propagation in concrete, the effectiveness of epoxy repair on concrete, and the variety of experimental methods to be used in this study.

Chapter 3 of this thesis summarizes the experimental methods, specimen, and results of the concrete cylinder experiments. This included both the plain and epoxy-repaired specimen.

Chapter 4 describes the summarizes the experimental methods, specimen, and results of the mortar experiments.

Chapter 5 contains the summarizes the experimental methods, specimen, and results of the beam experiments. This includes both “as-built” and epoxy-repaired specimen.

Chapter 6 explains the conclusions of this thesis.

The Appendices contain drawings of the experimental setups, and additional information regarding products used the experiments, and results from individual experiments.

References include the works cited in this thesis.

CHAPTER 2. LITERATURE REVIEW

To calibrate the XFEM and DEM models, sufficient data on their predictions of crack propagation and effects of epoxy repair are necessary. To collect this data, an effective experimental approach and test matrix must be designed. In order to properly develop the experimental approach and test matrix, knowledge about the fracture mechanics of concrete, the effect of epoxy repair, and previous test methods to find the necessary concrete characteristics used in literature. As a result, this literature review will cover three areas of study: (1) fracture mechanics and crack propagation in concrete, to understand development of longitudinal cracks in prestressed concrete; (2) the effectiveness of epoxy repair on concrete, specifically a high molecular weight methacrylate epoxy; and (3) the variety of experimental methods to be used in this study and their benefits, drawbacks, and influencers.

2.1 Crack Propagation in Concrete

Since the research thesis' goal is to evaluate and calibrate two computer models regarding crack propagation and repair in concrete, a literature review into fracture mechanics and crack development is needed.

2.1.1 Development of Longitudinal Cracks in Prestressed Concrete

Since the 1960's, longitudinal cracks in prestressed concrete have largely been assumed to be caused by tensile stresses. Gergely and Sozen's (Gergely and Sozen, 1967) analytical model demonstrated that the internal stress distribution of a prestressed girder is not sufficient to resist the prestressing force at the end of girders. The induced internal

reaction moment results in tensile stresses, which create longitudinal cracks (Gergely and Sozen, 1967). Figure 2 illustrates the Gergely-Sozen model.

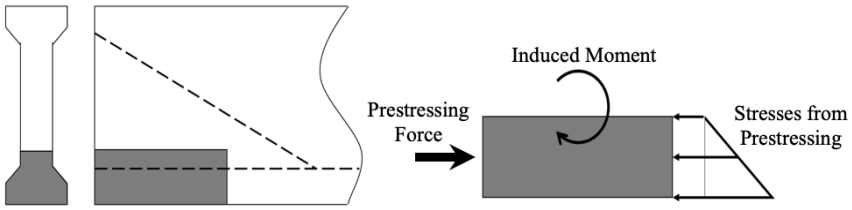

Figure 2: Gergely-Sozen Model for Stresses at End of Girders (Myers et al., 2001)

Both Gamble and Kannel et al. showed that the Gergely-Sozen model could predict the location of the cracks observed on prestressed girders from Illinois and Minnesota in 1997 (Gamble, 1997; Kannel et al., 1997).

To better understand the reason for the propagation of these longitudinal cracks, fracture mechanics models are used to understand the fracture at a smaller scale.

2.1.2 Fracture Mechanics of Concrete

Fracture mechanics is the study of the failure of a material based on the interaction between the applied stresses, preexisting cracks or defects, and material properties (van Mier, 2012). Originally proposed in the 1920 by Griffith, the concept of fracture mechanics was defined by the idea that remote loading of a material with pre-existing flaws will induce localized stress concentrations at the flaws, causing them to grow until the material fails (Griffith, 1920). One of the key components of fracture mechanics are the three modes of crack propagation: Mode I, or tensile opening; Mode II, or in-plane shearing; and Mode III, out-of-plane shearing (van Mier, 2012). When the failure is a combination of the three modes, the failure is called “mixed-mode.” The three modes are illustrated in Figure 3.

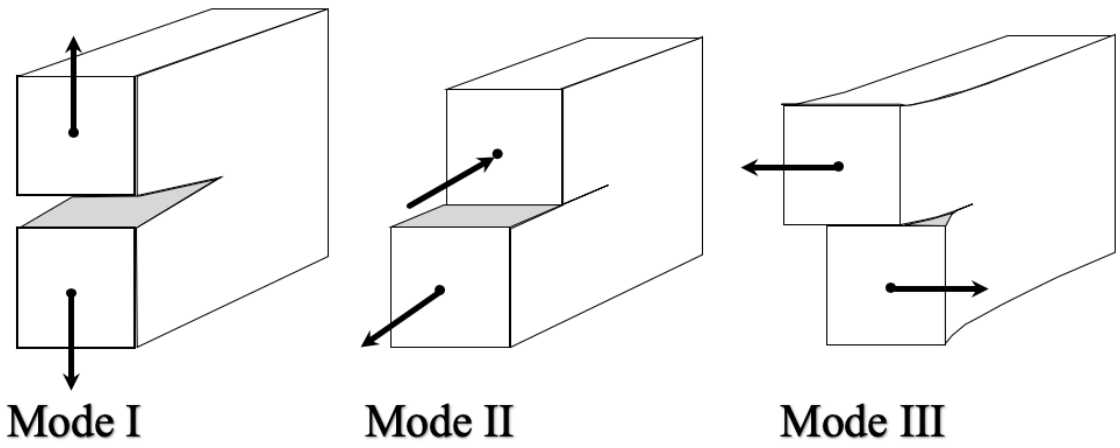

Figure 3: Modes of Fracture: (a) Mode I: Tensile opening, (b) Mode II: In-plane shearing, and (c) Mode III: Out-of-plane shearing (van Mier, 2012)

Since tensile cracking is of primary concern for concrete, including the longitudinal cracking that is the focus of this research, Mode I cracking was the main failure mode considered in the following work.

There have been multiple models that explain fracture mechanics of concrete. Most models consider a pre-existing crack in a linear elastic material with a nonlinear plastic section at the tip of the crack (van Mier, 2012). In the plastic region, relationship between the energy required to cause the crack extension and time is nonlinear. Concrete is unique in that the nonlinear zone is dominated by the fracture process, characterized as the breaking of atomic bonds, rather than the plastic deformation seen in ductile failures.

A widely accepted model is the Fictitious Crack Model (FCM) by Hillerborg et al. (Hillerborg et al., 1976). This model contains a cohesive zone, where cohesive stresses cause the atomic bonds at the crack tip to rupture and the crack to extend. A diagram of the FCM is shown in Figure 4.

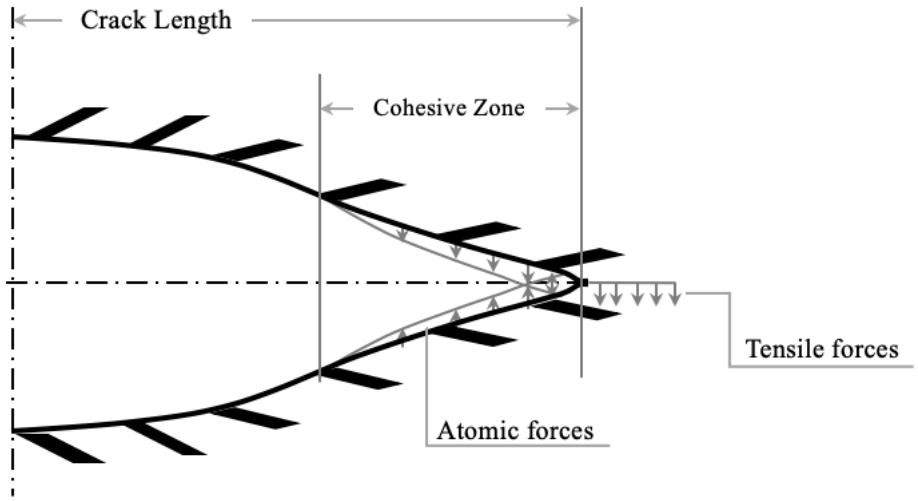

Figure 4: Cohesive Segment Diagram as proposed by Hillerborg et al. (Hillerborg et al., 1976)

The FCM provides understanding of the fracture at the crack tip and the additional development of microcracks in the cohesive zone, which all eventually lead to crack growth (van Mier, 2012). The basis of this fracture mechanics model stems from a focus on the fracture energy, or the energy required to initiate a crack in concrete. The fracture energy is quantified as the area under the tensile stress versus the crack opening curve, also known as the softening curve. In this research thesis, the XEFM cohesive segment model compared a linear and bilinear approximation of the softening curve so as to predict crack propagation.

The fracture mechanics of concrete is further complicated on the phase level of concrete. Although the FCM model can approximate the mechanics on the microscale, as the scale increases, the propagation becomes more difficult to assess, partly because the presence of aggregates in the matrix leads to alterations in the fracture mechanics.

2.1.3 Effect of Aggregates in Mortar Matrix

To understand how to assess the strength of concrete, concrete can be modeled using three phases: mortar matrix; aggregate; and the interfacial transition zone (ITZ) (van Mier, 2012).The mortar matrix is comprised of the hydrated cementitious material and fine aggregate. Although coarse aggregates increase strength due to particle interlock, coarse aggregates introduce a larger interfacial transitional zone (ITZ) phase in the concrete. Traditionally, the ITZ is the weakest phase of concrete as the cementitious material is not fully hydrated near the interface with the aggregate. This region is primarily characterized by its porous structure of ettringite and calcium hydroxide (CH) crystals rather than fully hydrated cement particles as shown in Figure 5. The ITZ is significantly weaker than the mortar phase or the aggregate phase in concrete. As the weakest phase, crack propagation typically passes through the ITZ. As a result, at a given water to cement ratio, mortar is typically stronger than the corresponding concrete because of the absence of the weak ITZ induced by the presence of coarse aggregates (Alexander and Mindess, 2005; Mehta and Monteiro, 2006).

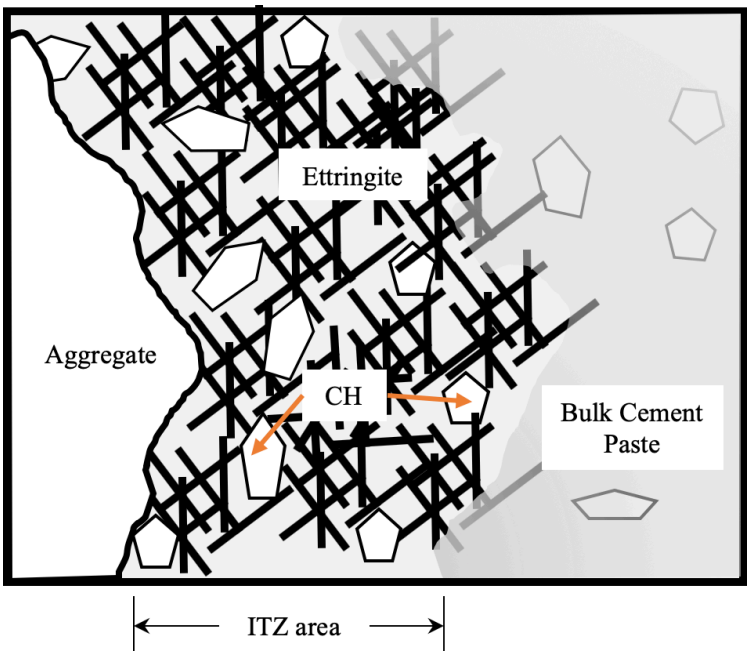

Figure 5: Diagram Representation of the ITZ (Mehta and Monteiro, 2006)

Since aggregates affect the fracture process by influencing the size of the ITZ, understanding how aggregates affect crack propagation is important for this research. The presence of aggregates and their effects on the crack propagation depend the aggregate type, surface texture, and shape. Aggregate type is determined by the aggregate's chemical makeup. Aggregates with certain forms of silica can interact with water to undergo an Alkali Silica Reaction (ASR) that produces a sodium silicate hydrate (N-S-H) gel. This gel expands volumetrically, causing new stress concentrations and microcracks that lower the strength of the concrete (Alexander and Mindess, 2005). Although this reaction is significant in understanding broader types of concrete cracking, ASR-effected concrete is out of scope of this research.

The surface texture of aggregates can also affect the fracture of concrete. The rougher the texture, the greater the stress concentrations in the concrete. Aggregates with a smooth or glassy surface texture lead to less microcracks during the shrinkage phase of

the concrete than aggregates with a rough or crystalline surface texture (Alexander and Mindess, 2005). On the other hand, rougher textured aggregates can also lead to better mechanical bonding between the aggregates and the matrix to improve mechanical properties of concrete (Kaplan, 1959). However, since the computer simulations only model fully cured concrete on a macroscale, further analysis into the surface texture effect on the fracture of concrete is out of scope of this research.

Aggregate shape can be defined by in terms of sphericity and roundness. Roundness is the average radius of the corners and edges of the aggregate to the maximum possible inserted circle. Roundness describes how sharp the edges of the aggregate are. An aggregate of low roundness is described as angular. A diagram of how to measure the roundness of an aggregate is shown in Figure 6a. Sphericity is a ratio of the nominal diameter of the aggregate to the maximum possible intercept. Sphericity also is defined by how closely the aggregate approximates the shape of a sphere. An illustrated comparison of sphericity and roundness is presented in Figure 6b.**Error! Reference source not found.**

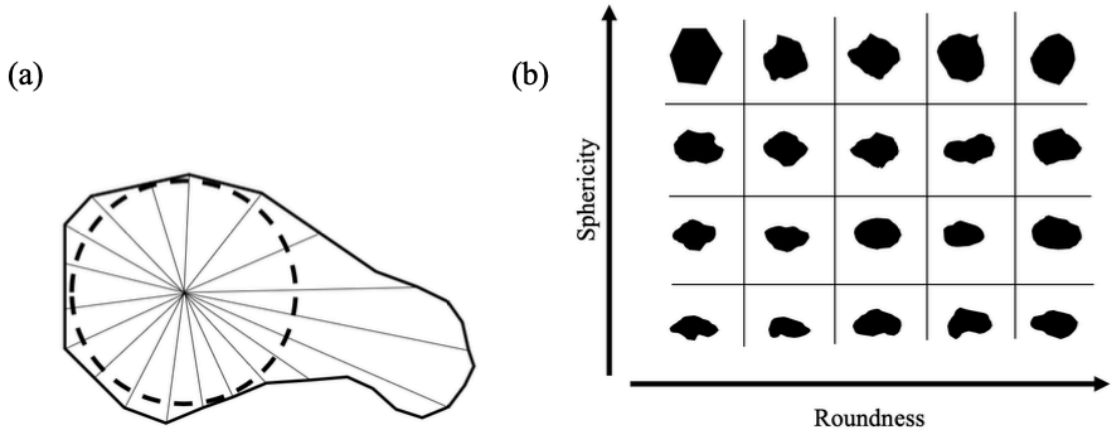

Figure 6: (a) Determination of Roundness of Aggregate (b) Sketches for assessment of sphericity and roundness of aggregates (Alexander and Mindess, 2005)

The aggregate shape plays a major part in determining how stress concentrations form within the concrete. Studies also show that the sphericity of aggregate can affect the fracturing of the concrete (Alexander and Mindess, 2005; Rocco and Elices, 2009). Rocco and Elices in 2009 illustrated how spherical and crushed aggregates cause differences in crack pattern - while cracks formed almost entirely at the interface of spherical aggregates, the crushed aggregates samples showed a more traditional crack pattern of failure. The differences in fractures can be seen in Figure 7.

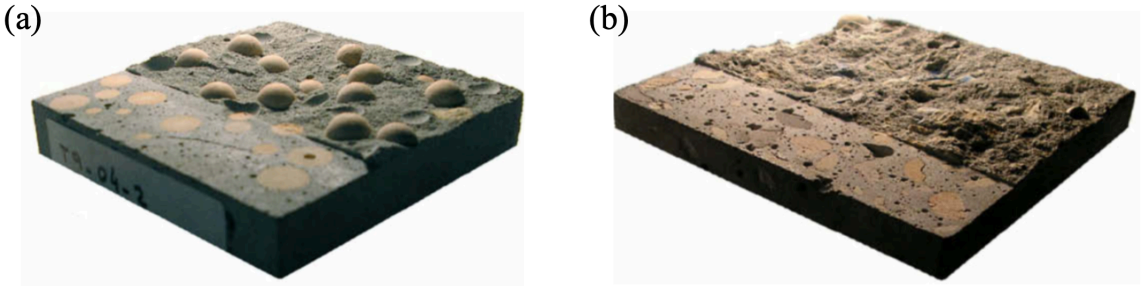

Figure 7: Fracture Surfaces of: (a) spherical aggregates; and (b) crushed aggregates (Rocco and Elices, 2009)

In addition, Akçaoğlu in 2017 used different shaped steel aggregates to determine that aggregates with sharp edges, such as a more angular aggregate, can lead to a higher stress concentration and microcracking within the ITZ. These microcracks formed around the sharp edges of the aggregates and appeared to lead to an increase in the crack propagation (Akçaoğlu, 2017).

2.1.3.1 Aggregates in Modelling

The work of Schlangen and Van Mier in 1992 created a computer simulation to determine the effect of the bond ITZ phase of concrete on the tensile strength. This

computer simulation used a triangle mesh and spherical aggregates (Schlangen and van Mier, 1992b, 1992a). The simulation, however, did not account for the effect of the realistic shape of aggregates on the fracture. In 2008, Van Mier then continued his research with Hau-Kit Man to create a three-dimensional lattice with realistic aggregates modeled using computer tomography (CT) scans of actual aggregates (Hau K. Man and van Mier, 2008). While this updated model had realistic and useful simulations, the model took a significant amount of time to produce results (Hau K. Man and van Mier, 2008; Hau Kit Man and van Mier, 2008). The DEM model calibrated with this research thesis, however, employs a three-dimensional model with realistic aggregate shapes without the expense of a long run time.

2.2 Epoxy Repair of Concrete

As the use and modeling of epoxy in cracked prestressed concrete was a main focus of this research, the following literature review sections focus on the use of epoxy as a repair method for concrete. A key factor in developing an experimental approach involving epoxy repair of concrete is choosing how to effectively apply the epoxy to the crack in the concrete. One epoxy application approach in the literature comes from the NCHRP Report 654 which recommends girder repair methodology based on the width of the longitudinal cracks (Tadros et al., 2010). The recommendations are listed in Table 1.

Table 1: NCHRP Report 654 Recommendation for girder acceptance based on longitudinal crack width (Tadros et al., 2010)

Longitudinal Cracks Width	*NCHRP report 654 recommends girders to be:*
< 0.012 in	Accepted
Between 0.012 in and 0.025 in	Repaired by Cementitious packing materials
Between 0.025 in and 0.050 in	Repaired by Epoxy Injection
> 0.050 in	Rejected and Replaced

Alternatively, the Precast/Prestressed Concrete Institute identifies three defect categories: those that can be accepted without repair, those that can be repaired, and those that must be rejected in their 2001 guide (PCI, 2001). The PCI guide has more detailed troubleshooting and repair procedures, depending on the location, orientation, length, and width of the cracks. It specifies a minimum width for epoxy repair beginning at 0.006 inches.

The both reports state that the epoxy should be injected into the crack with an applied pressure in correspondence to the manufacturer's specifications. The applied external pressure enables the epoxy to more effectively seep into the crack and thus achieve a more effective penetration into the concrete (PCI, 2001; Tadros et al., 2010).

In addition, a great amount of crack preparation needs to be done before the epoxy can be applied. The crack needs to be fully cleared all debris such as dirt, dust, or oil using high-pressured air. Injection ports are then periodically placed along the crack before a sealing material is applied to the remaining length. Finally, the epoxy is injected into the

crack under pressure from the injection machine (Keane, 2009b). A simplified diagram of this process is presented in Figure 8.

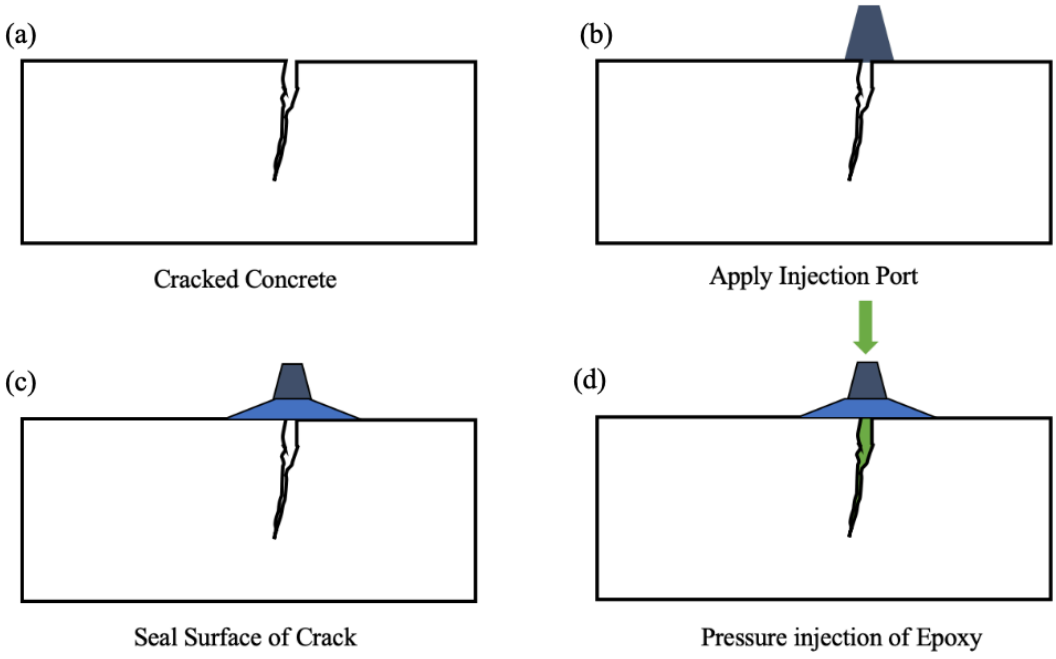

Figure 8: Simplified diagram of the pressure injection of epoxy procedures: (a) Prepare cracked concrete (b) Apply injection ports along the cracked surface (c) Seal the surface of the crack and around the injection ports (d) Inject the epoxy through the ports into the crack using a pressurized machine (Keane, 2009b)

Another method of epoxy injection is to use low viscosity epoxies, which fill and coat the cracks due to gravity. With the gravity filling method for epoxy crack repair, the epoxy seeps into the cracks before curing and stiffening to bind the epoxy and crack. However, it should be noted that gravity-fed epoxies are not effective in repairing moving cracks as this type of epoxy cannot act as a flexible joint (Issa and Debs, 2007). According to ACI RAP-2, gravity-fed epoxy repair methods should first fill the crack and then bond the concrete sides of the crack (Keane, 2009a). Literature evidence suggests that gravity-fed epoxies can help recover about 30% of the compressive strength capacity of a concrete cube (Issa and Debs, 2007). The Issa and Debs study on how a gravity-fed epoxy repair

approach worked for three different cubes is shown in Figure 9 (Issa and Debs, 2007). The experiment done by Issa and Debs first tested the capacity of an intact cube of concrete as shown in Figure 9a. It then tested the capacity of a cube with pre-existing end cracking as shown in Figure 9b. Finally, the experiment tested the capacity of a cube which had similar cracking to the previous cube, but had been repaired using epoxy as seen in Figure 9c. For gravity-fed epoxy repair systems, the viscosity is an important factor because epoxies of lower viscosities and higher molecular densities are more efficient in filling the crack when gravity is the only driving force.

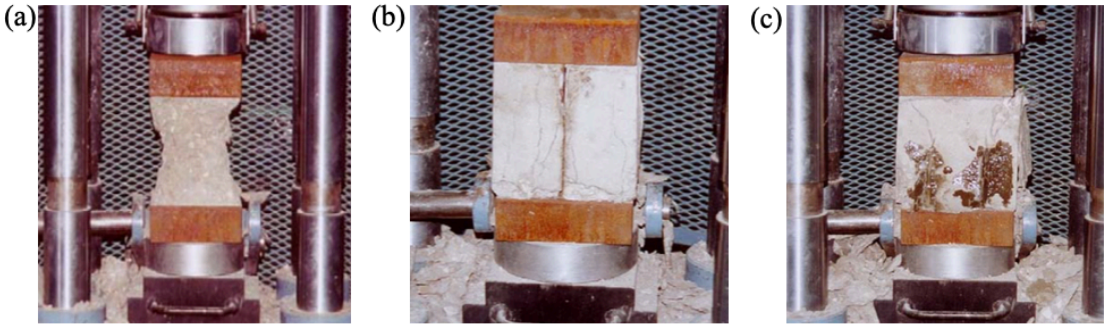

Figure 9: (a) crushed intact concrete (b) crushed pre-cracked concrete (c) crushed epoxy-repaired concrete (Issa and Debs, 2007)

In addition to how the epoxy is applied and the epoxy's viscosity, epoxy-repaired concrete is also dependent on the strength of the interface between the concrete and the epoxy. The interface is important because if a concrete structure is further stressed after repair, it is likely that new fractures will occur in the epoxy itself and/or the interface between the concrete and epoxy. There are a few methods to test the tensile strength of the interface between the concrete and epoxy. One is the ASTM C1583 test, the standard test method for "Tensile Strength of Concrete Surfaces and the Bond Strength or Tensile Strength of Concrete Repair and Overlay Materials by Direct Tension." This test is suitable

for epoxy overlay materials such as Fiber Reinforced Polymer (FRP) laminates attached to concrete by epoxy (ASTM C1583, 2013). Another means to test the tensile strength of the interface between the concrete and epoxy is based on the experimental study performed by Coronado and Lopez (Coronado and Lopez, 2008). This study fabricated splitting tensile test specimens to be tested following ASTM C496 procedures. After testing, the specimens were visibly assessed to determine if failure occurred in the concrete or along the concrete-epoxy interface. An illustrated example of the splitting tension failure seen in the study is shown in Figure 10a. In addition to the splitting tension samples, the Coronado and Lopez study also tested unreinforced notched beams to determine the fracture energy and failure location of repaired concrete. These beams were designed after the Hillerborg notched beam design (Hillerborg, 1985). The study found that the fracture energies of the repaired concrete was 64% higher than the fracture energy of plain concrete. The two failure modes observed were cracking along the interface and cracking within the concrete, as shown in Figure 10b and Figure 10c respectively.

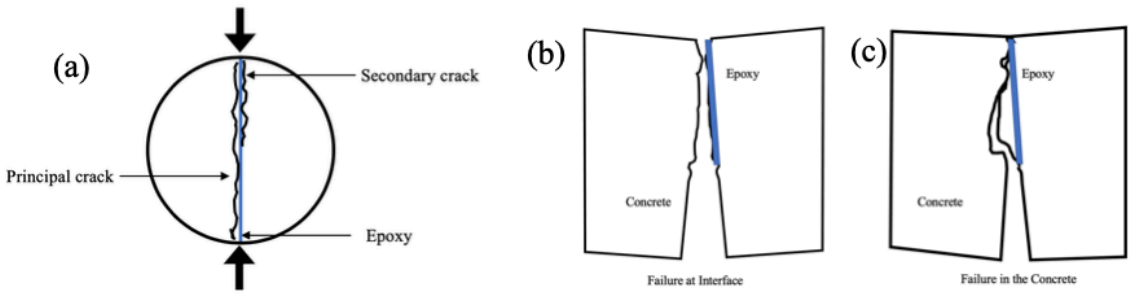

Figure 10: adapted from (Coronado and Lopez, 2008): (a) Sketch of Splitting Tension Failure Mode; (b) Sketch of notched beam failure at Epoxy-Concrete interface; and (c) Sketch of notched beam failure within the concrete

The epoxy used in this thesis was the Transpo Industries Sealate T-70 High Molecular Weight Methacrylate (HMWM) resin material. The material is a three-part

mixture of proprietary Sealate resin, Cobalt Nathenate promoter, and a CHP initiator. This epoxy has a very low viscosity of less than 20 cps and low surface tension, which allows it to penetrate thin cracks (Transpo Industries, 2017a). Thus, HMWM resin is noted as being an excellent choice for sealing cracks that employ the gravity-fed method and is recommended by sixteen different departments of transportation across the United States (Rahim et al., 2010). In terms of crack width, HMWM material can be used to seal cracks as narrow as 0.05 mm and as wide as 12.7 mm (Rahim et al., 2010). Finally, a study into different types of HMWM monomers used to repair cracked concrete showed that the use of HMWM was able to fill hairline cracks and increased the stiffness of cracked flexural members (Rodler et al., 1989).

For this research thesis, the experimental approach for epoxy repair employed gravity-fed as the injection approach, the Coronado and Lopez experimental method to understand the tensile strength of the interface, and a HMWM material as the low viscosity epoxy.

2.3 Experimental Techniques

Since a main objective of this research was development of experimental methods to calibrate the computational models, the following literature review sections focus on the test methods that evaluate compressive behavior, tensile behavior, and the fracture propagation of plain concrete, repaired concrete, and mortar.

2.3.1 Uniaxial Compression

To understand and quantify the compressive behaviour of the plain concrete, a uniaxial compression experiment was used. In this experiment, compressive strength can

be found by uniformly loading a sample axially until failure. The strength is defined as the ultimate compression load per cross-sectional area. Compressive strength is typically found using cubical or cylindrical samples. The use of cubical specimen is prevalent in Europe while cylindrical samples are standard in the United States, Canada, and Australia. The standard cylinders' size is 6 inch x 12 inch, although other sizes are permitted. This research used ASTM C39 procedures to determine the compressive behaviour of plain concrete. When loaded in uniaxial compression following ASTM C39, concrete typically fails in one of the six fracture patterns, illustrated in Figure 11.

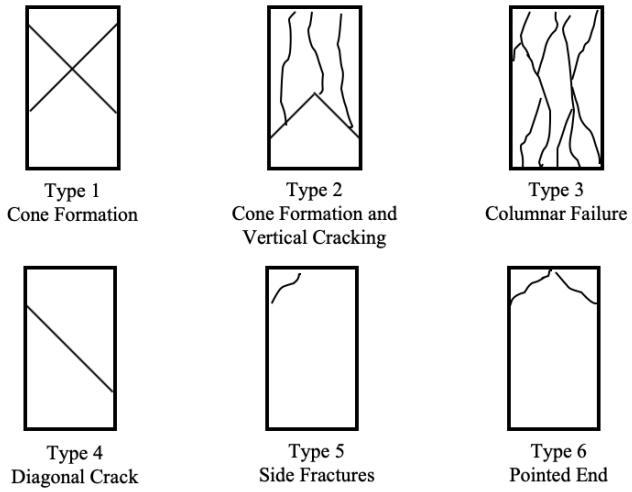

Figure 11: Schematics of typical uniaxial compression fracture patterns (ASTM C39, 2016)

2.3.2 Split Cylinder/Brazilian Test

One of the most widely used methods to determine the tensile strength of concrete is the split cylinder test. The split cylinder test, sometimes known as the Brazilian test or Splitting Tension test, was developed by Professor Fernando L.L.B Carneiro and presented at the 5th meeting of the Brazilian Association for Technical Rules in 1943 (Mehta and Monteiro, 2006). The experiment involves applying a vertical compressive force

perpendicular to the cylindrical axis of the sample. The load is increased until the cylinder ruptures. Figure 12 illustrates the test set up and schematics of the split cylinder test. The methodology and procedures of the test that were followed in this research were that of ASTM C496 (ASTM C496, 2017).

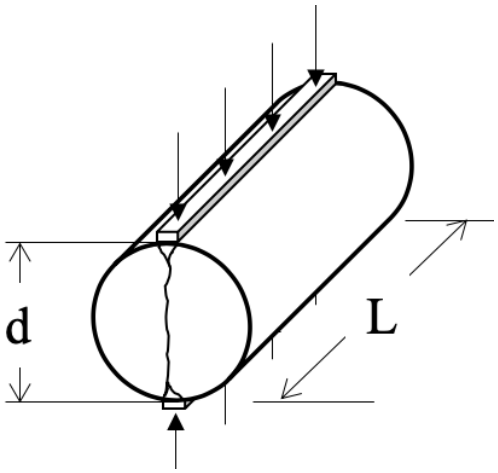

Figure 12: Splitting tension test schematic

From this setup, the tensile strength is thus assumed to be governed by linearly elastic behavior as stated in Equation 1.

$$f_{st} = \frac{2P}{\pi L d} \qquad \text{Equation 1}$$

Where f_{st} is the ultimate splitting tensile strength, P is the maximum applied load as indicated by the testing machine, L is the length of the cylinder, and d is the diameter. For this research, the split cylinder test is used to determine the tensile strength of plain concrete, repaired concrete, and mortar. In addition, through the use of a slow-motion camera, the crack propagation of the tension failure will be recorded for visual analysis of the fracture. The camera used for the experiments is a Sony RX10 Digital camera, which is capable of filming 1,000 fps during a four second period of time. Further details on the experiment are given in Chapter 3.

Although the split cylinder test can approximate the tensile strength of concrete, due to the test's inherent instability and nonuniform stress gradient it does not capture an accurate softening response (van Mier, 2012). As a result, an additional indirect tension test is needed to determine the fracture energy, as required for the fracture mechanics model.

2.3.3 Three Point Bend Test for Indirect Tension

To determine the fracture energy of the concrete, a specialized three-point bend test on a notched beam is used. This test was derived from Hillerborg and others' experiments during their development of the FCM (Hillerborg, 1985). A diagram of the fracture energy three-point bend test proposed by Hillerborg is shown in Figure 13. With some geometric design variations, multiple past studies successfully used this method to find the fracture energy of concrete (Bazant, 1992; Lee and Lopez, 2014). For this research, it was determined that size of the samples used would impact the results, so it was necessary to consider the size effect.

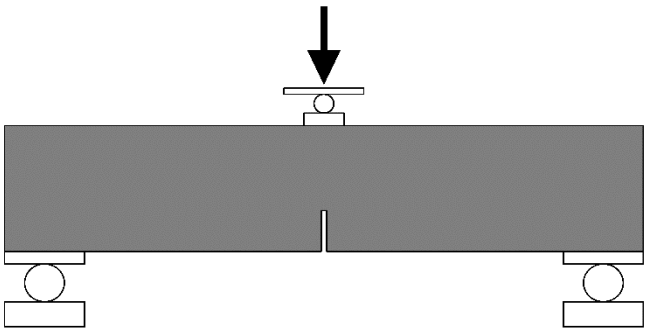

Figure 13: Notched Three Point Bend test to find Fracture Energy

The results of the three-point bend test for notched beams are dependent on the size, shape, and self-weight of the beam. Previous studies have shown that the three-point bend

test on notched beams exhibits an increase in fracture energy with increasing size. One possible solution to this issue is the size-effect method (van Mier, 2012). Size effect is a phenomenon in which large-scale structures exhibit weaker tensile strength than smaller laboratory studies.

2.3.4 Three Point Bend Test for Flexure

In addition to testing the properties of plain concrete, repaired concrete, and mortar, the research also required that the experimental approach examine the crack propagation and repair recovery capabilities of the epoxy on reinforced concrete. As a result, a three-point bend test was performed on reinforced concrete. This test was designed to examine the impact of epoxy repair on the capacity of reinforced concrete. A simplified diagram of the test is illustrated in Figure 14.

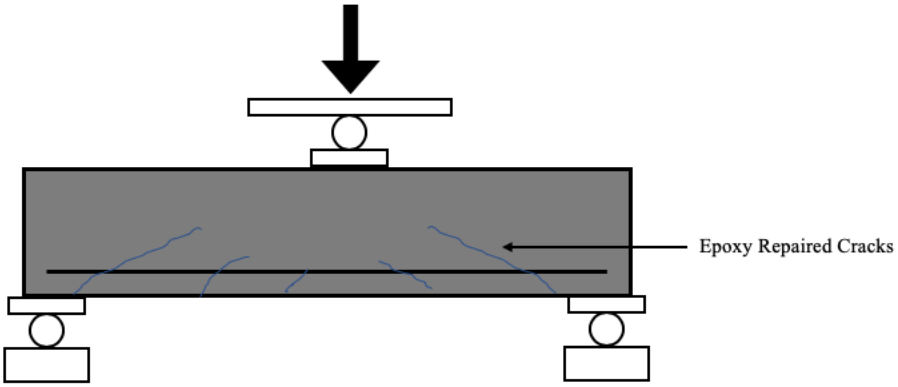

Figure 14: Epoxy-repaired Reinforced Beam Three Point Bend Test

Larger scale tests have been performed on reinforced concrete beams repaired with epoxy (Bertero et al., 1973; Ahmad et al., 2013). These tests repaired cracks using the epoxy injection method with an epoxy that had a higher viscosity than the one used in this research. As a result, this experiment focused on understanding the repaired capacity of a

simply supported reinforced concrete beam repaired with a High Molecular Weight Methacrylate using the gravity filling technique.

2.3.5 Other available tension tests

Other methods to evaluate the tensile strength of concrete exist in addition to the split cylinder and indirect three-point bend test. These include a uniaxial tensile testing method designed for use in ERDC's Pressure Vessel for triaxial testing (Reichard, 2015). This method uses a uniaxial loading machine, LVDT's, and a small cylindrical sample glued into connections using epoxy. The sample is loaded axially in tension until failure. It should be noted that this method was performed on Ultra High-Performance Concrete. A simplified diagram of the uniaxial tensile test is shown in Figure 15a. The second alternate method was the Wedge Splitting Test, which provides an estimation of the fracture energy of concrete. The test uses a cube of concrete with a notch section. A wedge is placed into the notch and the loaded until the concrete fails (Linsbauer and Tschegg, 1986; Löfgren, 2004; van Mier, 2012). A simplified diagram of this test is illustrated in Figure 15b.

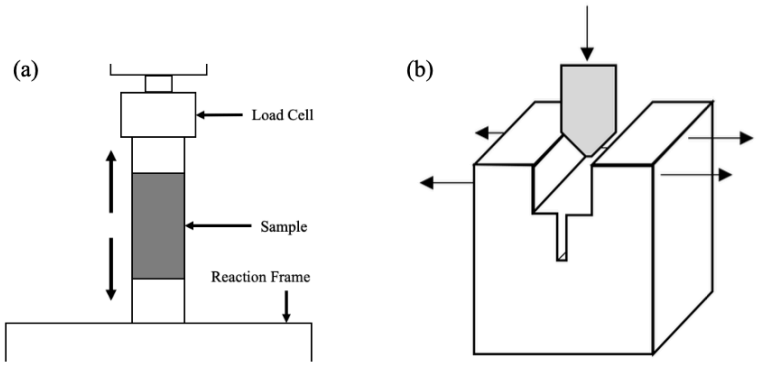

Figure 15: (a) Simplified Diagram of Uniaxial Tensile Test (b) Wedge Splitting Test

CHAPTER 3. CONCRETE CYLINDER EXPERIMENTS

The experiments presented in this chapter are divided into two categories: plain concrete cylinder experiments (Section 3.1) and epoxy-repaired concrete cylinder experiments (Section 3.2).

3.1 Plain Concrete Experiments

Cylinders of plain concrete comprised the majority of the experiments that were performed. These experiments were conducted to provide both compressive and tensile data to calibrate the parametes of the plain concrete cohesive segment model.

3.1.1 Specimen Size Selection

Four initial concrete cylinder experiments were conducted to determine the specimen size as well as to refine the experimental protocol. Experiments were conducted both in tension via splitting and uniaxial compression. Splitting tension experiments, sometimes referred to as the Brazilian test (see Section 2.1.4), were initially performed on 4 inch x 8 inch cylinder specimens. The concrete behaved as expected in terms of strength, but upon visual inspection of the specimens after failure, it was noticed that the fracture occurred off-center. A primary crack formed from the side of the bearing strip and a secondary crack formed on the opposite side of the bearing strip, as shown in Figure 16. Evidence from the literature suggests that the cause of the off center cracking is from the ratio of bearing strip width to specimen diameter (Coronado and Lopez, 2008).

The initial tensile splitting tests were also used to verify the ability to capture high speed video of the crack propagation through the face of the sample. These initial tests indicated that the fracture of the 4 inch x 8 inch cylinders happened too quickly for the

1,000 frames per second (fps) high-speed camera to capture quality data. From the literature, it was found that many experiments used 6 inch x 12 inch cylinders to monitor the crack growth with such cameras (Ross et al., 1996; Li, 2004). As a result, it was determined that 6 inch x 12 inch cylinders would be used for for future experiments in the study in order to ensure and monitor symmetric crack propogation.

Figure 16: Undesired tensile splitting failure of initial 4 inch x 8 inch plain concrete specimen.

3.1.2 Materials

The concrete used in these experiments was made by Thomas Concrete and followed the GDOT Specification for pre-stressed concrete (GDOT et al., 2013). The concrete provided by Thomas Concrete had mixture weight fractions and properties are listed in Table 2. In addition, upon arrival, the concrete mixture had the properties as listed in Table 3.

Table 2: Concrete mix used in concrete cylinder experiments

Material	***Weight Fraction***
Cement	18.4%
Water	6.5%
Coarse Aggregate	47.1%
Fine Aggregate	28.0%

Table 3: Properties of concrete used in concrete cylinder experiments

Property	
Water-cement ratio	*0.3545*
Cement Type	*Type I*
Slump	*3.25 inch*
Specific Gravity (Course Aggregate)	*2.71*
Specific Gravity (Fine Aggregate)	*2.69*

The composition of the coarse aggregate was granite-gneiss aggregate from Norcross, Ga distributed by Vulcan Materials Company. The coarse aggregate used was size 67. The granite-gneiss aggregates are formed as a banded combination of an igneous rock (granite) and its metamorphic rock counterpart in gneiss. Both rocks are primarily composed of strained and microcrystalline quartz. Given these various component parts, the rocks are susceptible to Alkali-silica reaction (ASR), which in turn, can cause microcracks in the concrete due to expansion of the ASR gel with water (Alexander and Mindess, 2005). For the purpose of this research, it was determined that the effect of ASR gel on crack propagation could be ignored.

Granite-Gneiss aggregates, as shown in Figure 17, can be classified as having a surface texture as crystalline, a sub-angular shape, and a low sphericity. Coarse aggregates' texture and shape can affect the presence of stress concentrations and the overal fracture mechanisms of the concrete. Therefore, scans of individual aggregate were conducted to create realistic and precise aggregate shapes for the computational models in order to facilitate better prediction of the location and timing of microcracks. A *Matter and Form 3D Tabletop Scanner*, as shown in Figure 18, was used to create three-dimensional point cloud files to generate realistic shapes of aggregate within the model. Examples of the point cloud aggregate scans from this research are shown in Figure 19.

Figure 17: Granite-Gneiss aggregate used in concrete cylinder mix

Figure 18: Matter and Form 3D Tabletop Scanner used for developing realistic aggregate models.

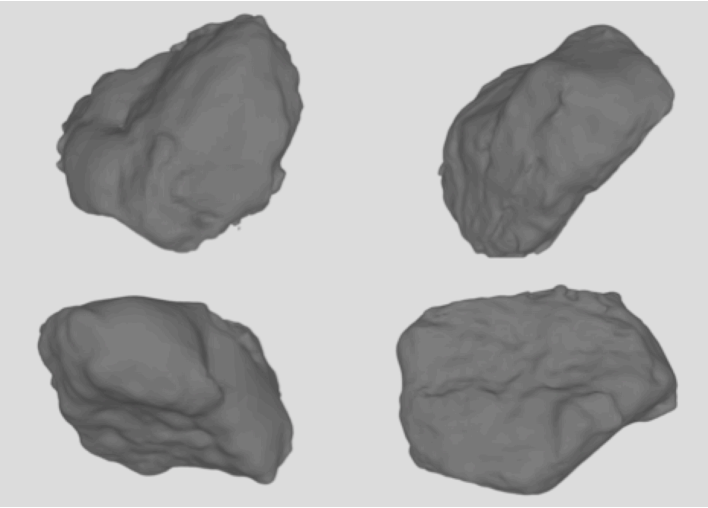

Figure 19: Point cloud renderings from aggregate scans.

3.1.3 Uniaxial Compression Experiments

As discussed in the literature review (Section 2.3.1), to understand and quantify the compressive behaviour of the plain concrete, a uniaxial compression experiment was used. This research used ASTM C39 procedures to determine the compressive behaviour of plain concrete. The SATEC PRISM MKIII-C machine with INSTRON 59-R7 controller located

at the Georgia Institute of Technology Structural Engineering and Materials Laboratory was used to conduct the uniaxial compression experiments. The experiments were conducted with a loading rate of 60 kips per minute. An example of the test setup is shown in Figure 20.

The plain concrete cylinder experiments are categorized in two groups. Group 1 is comprised of concrete samples that were cured and aged in a controlled fog room environment for the duration of their sample age. Group 2 is comprised of samples that were removed from the controlled environment at 56 days and were then allowed to age at ambient lab temperatures until their test date. Group 2 cylinders are the concrete cylinder samples used to determine the compressive strength of the concrete used for the beams tested (see Chapter 5). Therefore, these cylinders were removed from the controlled environment of the fog room in order to have the same aging environment and moisture content as those of the beams that were removed from the fog room at 56 days for storage. The compressive strengths of cylinders are reported in Table 4. Figure 21 shows the data graphically by group.

Figure 20: Uniaxial compression setup as outlined in ASTM C39.

Table 4: Summary of plain concrete cylinder average compressive strengths.

Sample Age (days)	*Compressive Strength, f'c (ksi)*	*Group Category*
28	4.72	1
49	4.68	1
74	5.17	2
95	5.13	2
104	5.03	2
112	5.13	2
119	5.06	2
133	5.66	2

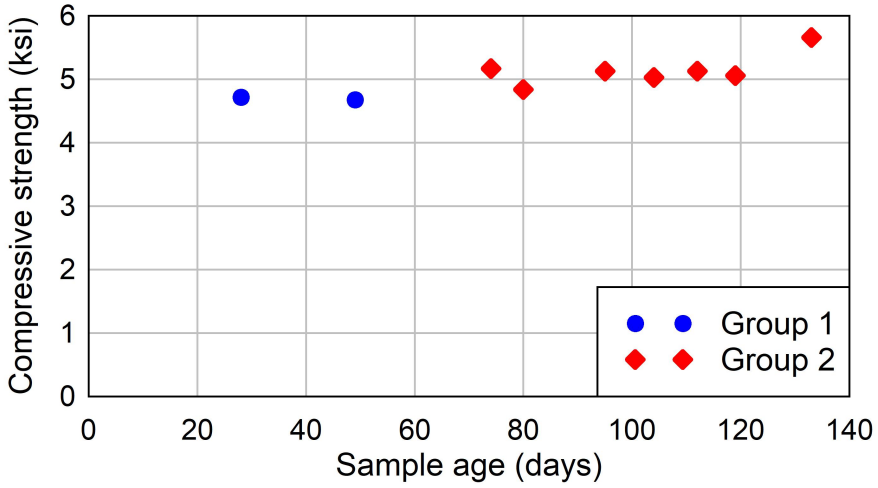

Figure 21: Concrete cylinder average compressive strength at different ages.

As discussed previously, the compressive strengths of the plain concrete cylinders were determined using ASTM C39 procedures. However, since the Group 2 samples were not at the standard moisture content, a slightly modified ASTM C39 procedure was used. This modification was the allowance of a lower than standard moisture content of the concrete cylinders in order to remain consistent with the beam experiments, which are presented in Chapter 5. Figure 22 illustrates the differences between the compressive stress-strain curves of the Group 1 and Group 2 samples. The Group 1 samples demonstrated a higher modulus of elasticity than the Group 2 samples. This difference is consistent with the literature (Reinhardt et al., 1990) that states that concrete with a higher moisture content can exhibit higher modulus as the moisture increases the stiffness of the concrete. The difference in compressive strength between Group 1 and Group 2 cylinders can also be attributed to the difference in sample age between the groups. All Group 2 samples were older than all Group 1 cylinders.

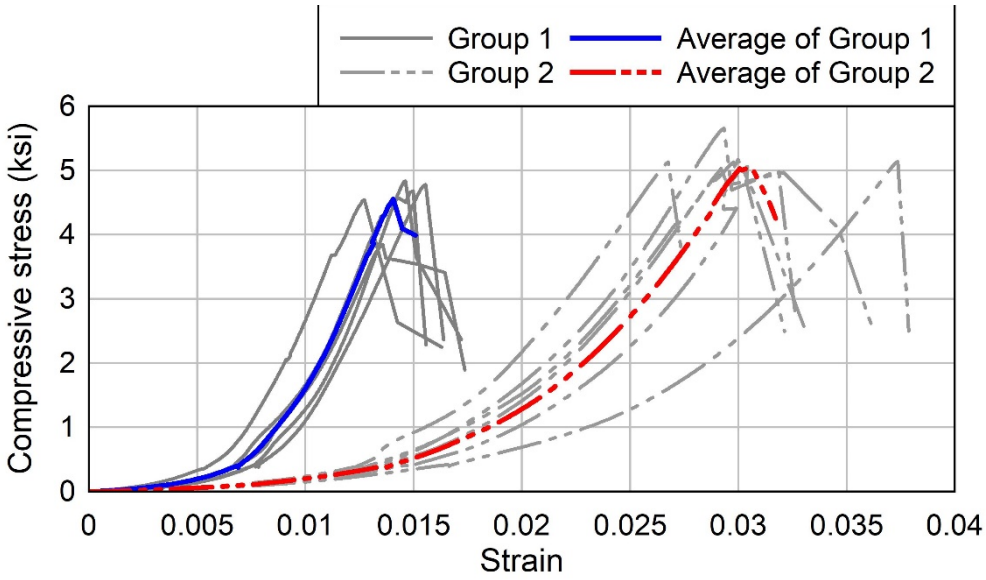

Figure 22: Compressive test results of plain 6 inch x 12 inch concrete cylinders

Although the two groups exhibited different stress-strain behaviors, both groups had similar failure modes. Utilizing the classifications given in Figure 11, the cylinders primarily demonstrated a columnar failure mode. A posttest photo showing the failure from an example experiment is given in Figure 23.

Figure 23: Typical plain concrete behavior indicative of a type 3 columnar failure.

3.1.4 Splitting Tension Experiments

As discussed in the literature review (Section 2.3.2), to determine the tensile strength of concrete, a split cylinder test was used in this research. The methodology and procedures of the test that were followed in this research were that of ASTM C496 (ASTM C496, 2017). For this research, the SATEC PRISM MKIII-C with INSTRON 59-R7 controller located at the Georgia Institute of Technology Structural Engineering and Materials laboratory was used to load the samples at 11.3 kips per minute. The experimental setup is shown in Figure 24.

Figure 24: Splitting tension experimental setup.

The splitting tension cylinder samples are categorized in the same way as for the uniaxial compression test samples. Group 1 is comprised of concrete samples that were cured and aged in a controlled fog room environment for the duration of their sample age. Group 2 is comprised of samples that were removed from the controlled environment at 56

days and were then allowed to age at ambient lab temperatures until their test date. As previously stated, Group 2 cylinders are the concrete cylinder samples used to determine the corresponding splitting tensile strength of the concrete used in the beams tested (see Chapter 5). Therefore, these cylinders were removed from the controlled environment of the fog room to have the same aging environment and moisture content as those of the beams, which were removed from the fog room at 56 days. Similar to the compressive strength test, the splitting tensile strengths of the plain concrete cylinders were found using ASTM C496 procedures. However, since the Group 2 samples were not at the standard moisture content, a slightly modified ASTM C496 procedure was used. The splitting tensile strengths of cylinders are listed in Table 5.

Table 5: Summary of plain concrete cylinder average ultimate tensile strengths.

Sample Age (days)	*Ultimate Tensile Strength (ksi)*	*Group Category*
28	*0.357*	*1*
49	*0.411*	*1*
104	*1.36*	*2*
112	*1.31*	*2*
119	*1.12*	*2*

Due to the different curing times and environments, the stress-strain behavior of Group 1 and Group 2 differ. The differences in the stress-strain behavior between Group 1 and Group 2 is illustrated in Figure 25. The Group 2 samples have significantly higher ultimate splitting tensile stress than the Group 1 samples. Although part of the increase of strength can be attributed to the age of the samples when tested, the differences in the initial slope indicate that the differences in moisture content likely affected the splitting tension strength. The lower moisture content of Group 2 likely affected the internal friction and

cohesion on the macroscopic scale of the concrete and contributed to the Group 2 samples' higher tensile strength. This is consistent with the work of Guo et. al, which suggest that the critical stress needed to fracture the concrete is lowered when the amount of water absorbed is increased (Guo and Waldron, 2001).

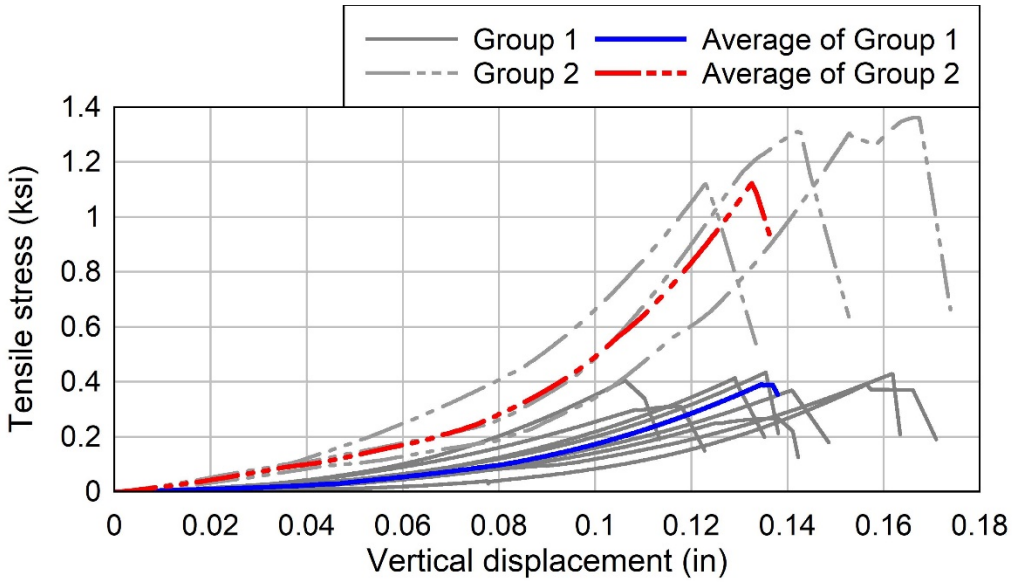

Figure 25: Splitting tension test results of plain 6 inch x 12 inch concrete cylinders.

In addition to the measurements taken by the testing machine (i.e., load and displacement), the tensile behavior was recorded for visual analysis of the crack propagation with a high-speed camera. A Sony RX10 Digital camera was used to monitor the fracture mechanisms. The camera was capable of filming 1,000 fps over a four second duration. The typical failure pattern and propagation from an example experiment is shown in Figure 26. Figure (a) denotes the crack initiation and is highlighted for clarity in red. Figure (b) shows the fully formed crack. Figure (c) shows the crack at the ultimate tensile stress. Finally, Figure (d) shows the specimen posttest.

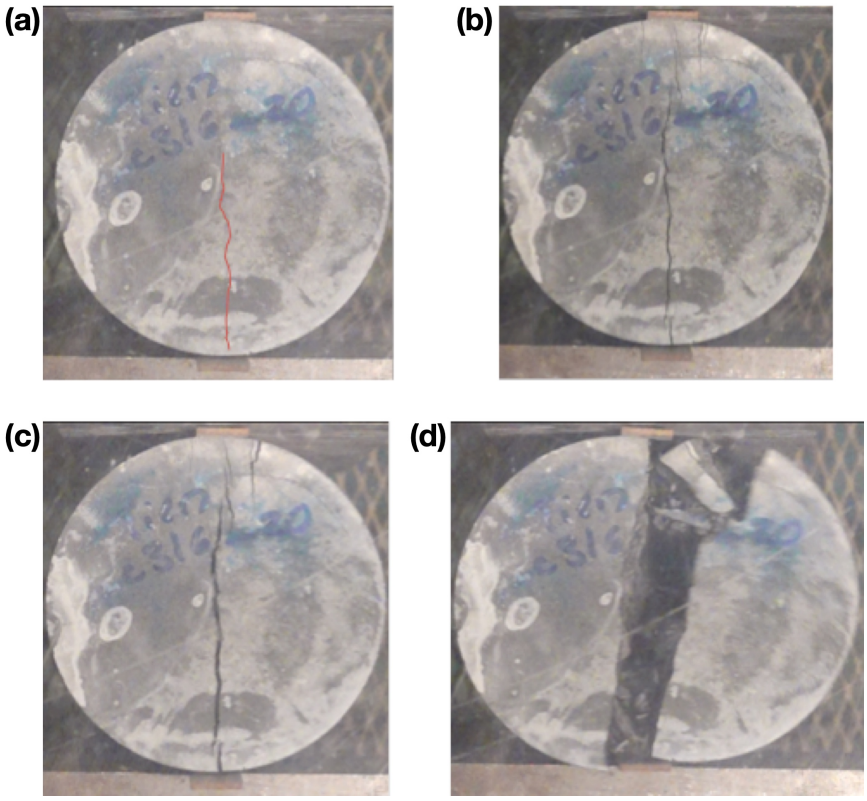

Figure 26: Example tension splitting crack propagation in plain concrete from high-speed camera: (a) crack initiation (highlighted in red for clarity); (b) fully formed crack (c) at failure; (d) post fracture.

As mentioned in the literature review in Section 2.3.2, that although the split cylinder test can determine the ultimate tensile strength of the specimen, it does not provide an accurate depiction of softening response. As a result, an additional indirect tension test was necessary to determine the required fracture energy needed for the fracture mechanics model. This method is discussed in Chapter 5.

3.2 Epoxy-repaired Concrete Experiments

In addition to the plain concrete cylinders, an experimental procedure was created to evaluate the models' ability to simulate epoxy-repaired concrete cylinders. The epoxy used was a Sealate T-70 High Molecular Weight Methacrylate (HMWM) by Transpo Industries (see Appendix C). This type of epoxy, recommended by GDOT for this research,

is used in situations with thin cracks requiring the gravity feed application type. Similar to the plain concrete experiments, the repaired concrete cylinders were tested in uniaxial compression and splitting tension to evaluate the strength and mechanisms of failure.

3.2.1 Specimens

In order to have a controlled cylinder geometry and design, plain concrete cylinders were modified such that they could be repaired with epoxy. Plain concrete cylinders were first cut on a tile cutter lengthwise as illustrated in Figure 27a and b. Then, in order to test the effect of cylinder size, some samples were cut into smaller sections. A series of 6 inch x 6 inch samples and 6 inch x 4 inch samples were developed by cutting the lengthwise cut cylinders again as illustrated Figure 27c and d.

Once cut, the two halves' faces were ground flat in order to have a smooth surface for bonding. Construction silicon caulk was then applied to the edges of the sides of the two halves and a slim cardboard spacer was placed at the top and bottom to create a "crack." The two halves were then pushed and tightened together using hose clamps, as illustrated in Figure 28. The silicon caulk was allowed to fully set for 24 hours.

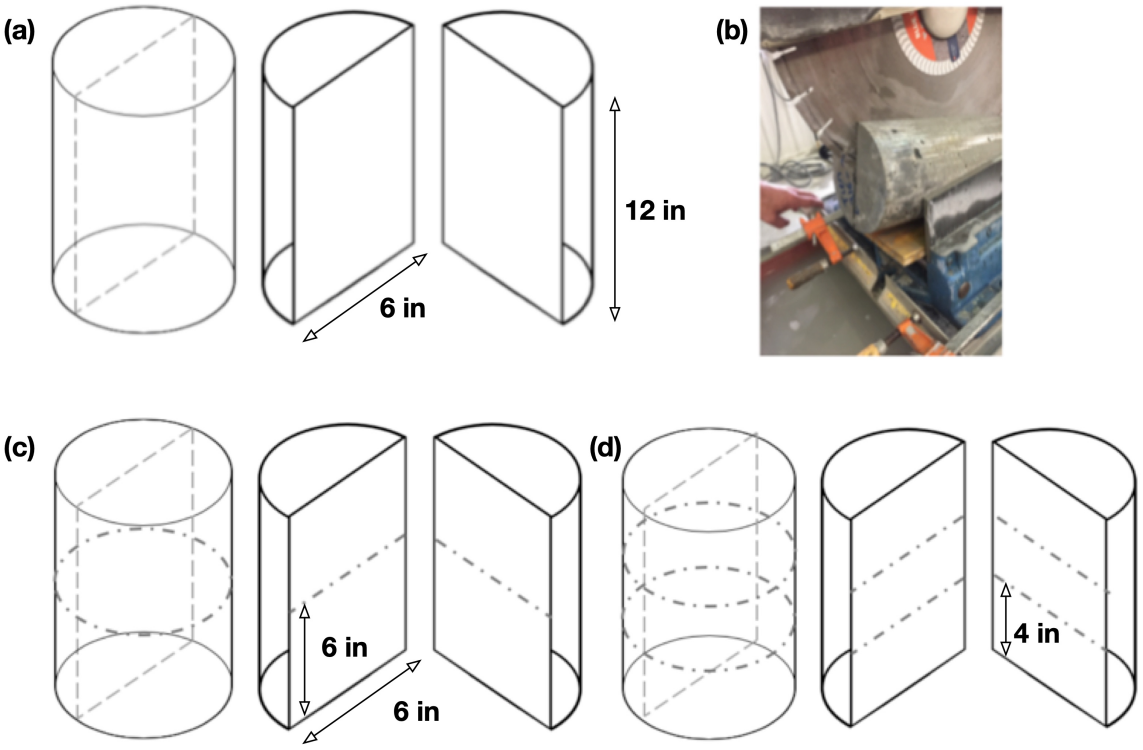

Figure 27: Epoxy-repaired specimen: (a) diagram of lengthwise cut on cylinders; (b) cutting of cylinder on tile cutter; (c) cut locations for 6 inch Samples; (d) cut locations for 4 inch samples.

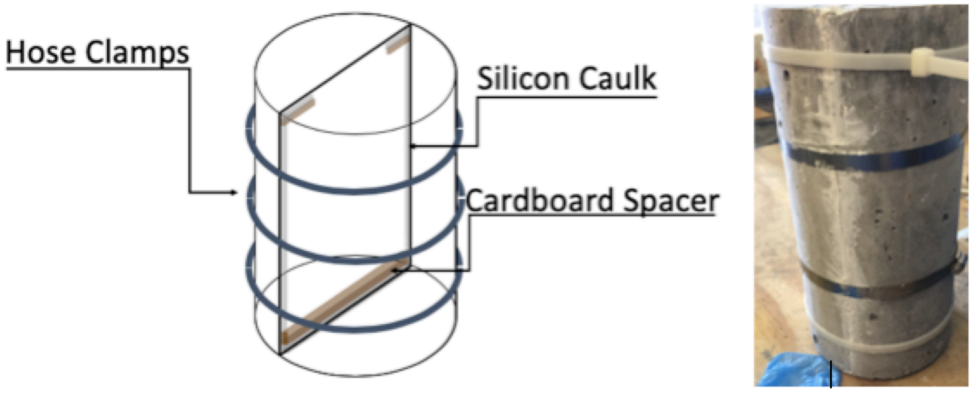

Figure 28: Preparation of epoxy-repaired cylindrical specimen prior to inclusion of epoxy.

The epoxy was a three-part mixture using three ingredients: Cobalt Napthenate promoter, CHP initiator, and propietary Sealate Resin. The ratio of the three ingredients were 75 mL : 150 mL: 1 gal, respectively (Transpo Industries, 2017b). The epoxy was created using the following steps:

1. The Cobalt Napthenate was measured out in clean gradient containers.
2. The CHP initiator was measured in its own container.
3. The resin was measured in its own container.
4. The resin was poured into a heatproof mixing container, as the reaction is exothermic.
5. The Cobalt Napthenate was added to the mixing container.
6. The mixture from steps 1-5 was then stirred for 2 minutes.
7. The CHP initiator was added to the stirred mixture and stirred again for 2 minutes.
8. The mixture was then in a pourable state for up to 15 minutes.

The epoxy was poured into the top opening of the sample until the newly constructed "crack" was completely full of High Molecular Weight Methacrylate as shown in Figure 29. The epoxy-repaired plain concrete was then allowed to cure for at least 48 hours before testing.

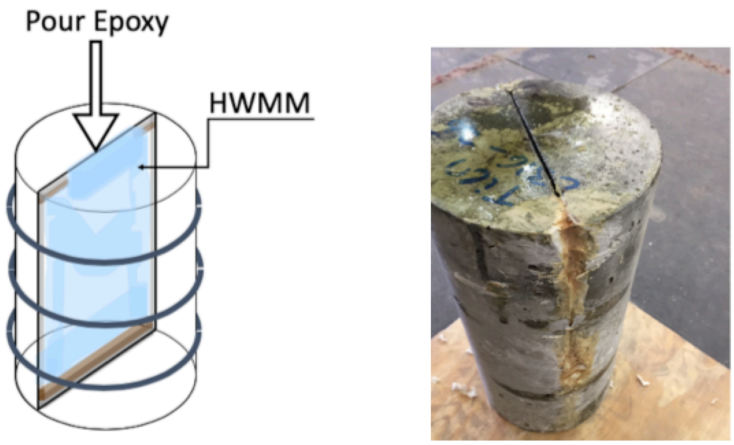

Figure 29: Preparation of epoxy-repaired cylindrical specimen - inclusion of epoxy.

3.2.2 Uniaxial Compression Experiments

Six inch x 12 inch epoxy-repaired concrete cylinders were tested in uniaxial compression. As these pre-repaired concrete cylinders were from the same batch as the plain concrete uniaxial compression cylinders, their sample age at testing was 153 days. Before modifications and repair, the concrete cylinders had cured and aged in the controlled fog room environment for 140 days. After epoxy repair was fully completed and the epoxy allowed to fully cure, the cylinders were tested in uniaxial compression following a procedure based on ASTM C39. This procedure used the same methodology as ASTM C39, but was performed on the repaired concrete cylinders so as to have comparable data as for plain concrete uniaxial compression experiments.

The stress-stain behavior of the epoxy-repaired cylinders in compression in comparison to the previously described Group 1 and Group 2 compression cylinders is shown in Figure 30. The epoxy-repaired concrete cylinders exhibited a similar elastic modulus as that of the Group 1 plain concrete cylinders. The similarity in modulus is likely due to the moisture content of the repaired concrete samples being closer to the moisture content of the Group 1 cylinders than the Group 2 cylinders. Using the interpolation of

Figure 21, it was determined that the approximate compressive strength of the concrete at 153 days is 5.5 ksi. The ultimate compressive strengths of the three repaired specimen are 5.49 ksi, 5.87 ksi, and 6.28 ksi, with an average of 5.88 ksi. It is assumed that the differences of strengths is associated with the the variability of concrete samples in compression, rather than with the epoxy repair.

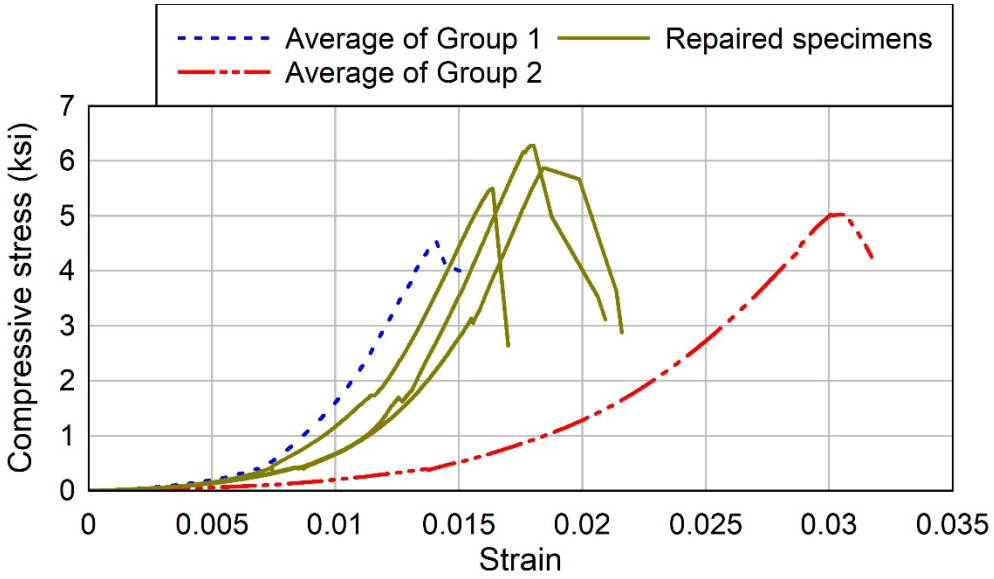

Figure 30: Compressive stress-strain behavior of epoxy-repaired specimens compared with plain concrete cylinder specimens of the same 6 inch x 12 inch size.

During the experiment, the epoxy-repaired cylinders first fractured along the epoxy-repaired spline as shown in Figure 31a and they then failed in a columnar failure mode as shown in Figure 31b. From high-speed camera photographs, it was noted that the repaired concrete cylinders fractured at the concrete/epoxy interface well before any fracture was noticed in the concrete itself. This outcome supports the conclusion that the compressive strength of the repaired concrete is very similar to the compressive strength of the plain concrete, since the early fracture of the epoxy-concrete interface does not affect the load transfer or contribute to any strengthening of the surrounding concrete, which dominates the response.

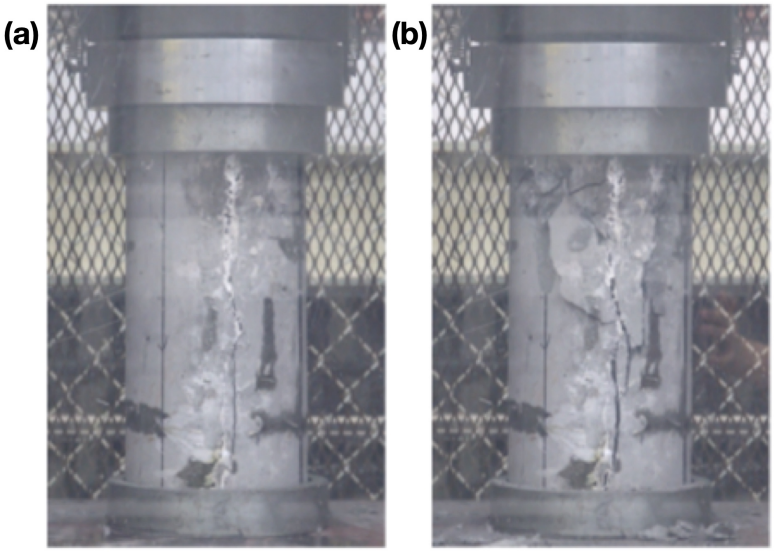

Figure 31: (a) Epoxy-repaired specimen at time 0:19; (b) compressive columnar failure at time 2:59.

3.2.3 Splitting Tension Experiments

Epoxy-repaired concrete cylinders were tested in splitting tension. As these pre-repaired concrete cylinders were from the same batch as the plain concrete splitting tension cylinders, their sample age upon testing was 153 days. Before modifications and repair, the concrete cylinders had cured and aged in the controlled fog room environment for 140 days. After epoxy repair was fully completed and the epoxy allowed to fully cure, the 6 inch x 12 inch splitting tension samples were tested following a procedure based on ASTM C496. This procedure used the same methodology as ASTM C496, but was performed on the repaired concrete cylinders so as to have data comparable to the plain concrete uniaxial compression data. The stress-stain behaviour of the epoxy-repaired cylinders in splitting tension in comparison to the previously described Group 1 and Group 2 samples is shown in Figure 32.

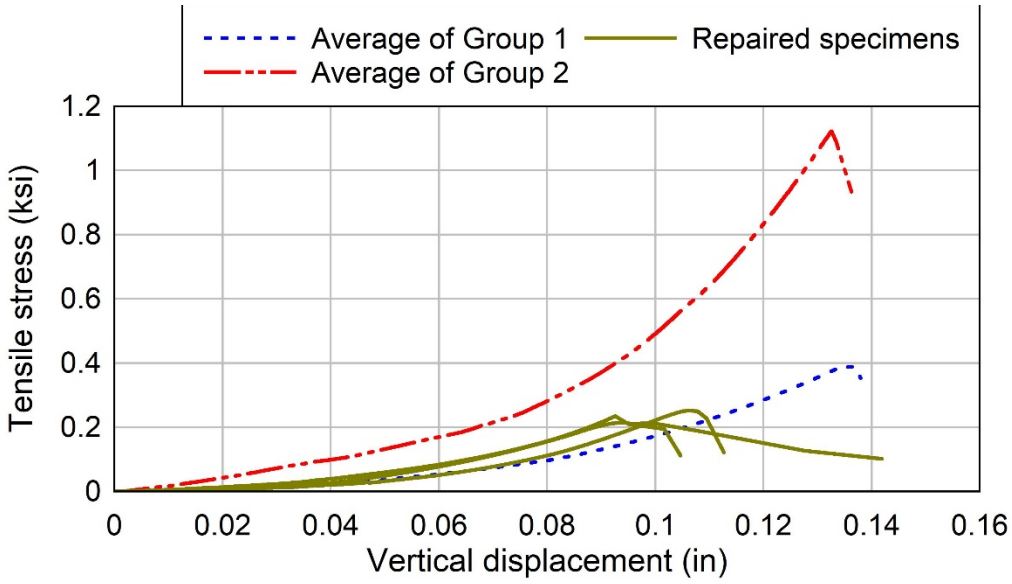

Figure 32: Splitting tension test results of epoxy-repaired cylinder specimens compared with plain cylinder specimens of the same 6 x 12 inch size.

The 6 inch x 12 inch splitting tension epoxy-repaired concrete specimen behaved similarly to the Group 1 plain concrete cylinders in terms of their elastic modulus. Like the repaired concrete compression samples, the repaired concrete tension samples had a moisture content more similar to the Group 1 plain concrete samples than to the Group 2 plain concrete samples. However, unlike the repaired concrete compression samples, the repaired concrete tension samples exhibited a visible decrease in tensile capacity in comparison to the Group 1 splitting tension plain concrete cylinders. This decrease in capacity is likely due to the weakness of the epoxy concrete interface in tension, which involved a smooth surface of the concrete. This theory is supported by the literature, in which is was noted that an increase of surface roughness of concrete subsequently increases the bond adhesion between the epoxy and the concrete due to the mechanical interlock that a roughened surface provides (Courard et al., 2014; Sadowski et al., 2016).

As with the plain concrete samples, a high-speed camera was used to capture the crack evolution of the repaired concrete in tension, which allowed for observational details

of when and how the epoxy-repaired concrete failed. This is of particular importance for the repaired concrete samples, because the post-test visual inspection did not clearly show the location of the failure initiation as opposed to the high-speed video, which demonstrated that the interface of the epoxy and concrete was the primary initial fracture location. The typical failure mechanisms of the repaired concrete specimens in splitting tension is shown in Figure 33.

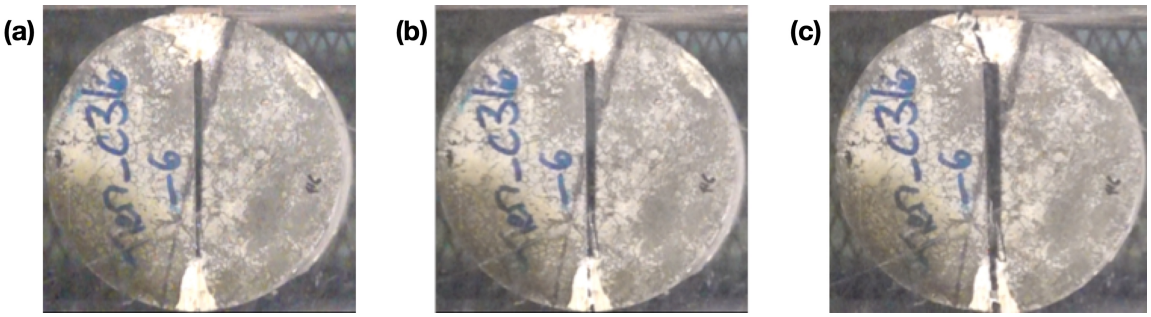

Figure 33: Repaired concrete tension behavior at interface: (a) before failure, (b) crack initiation, and (c) at failure.

3.2.4 Specimen Size Effect for Computational Efficiency

In order to evaluate the effect of sample size of the epoxy-repaired cylinders, six 6 inch x 6 inch and six 6 inch x 4 inch cylinders of epoxy-repaired concrete were tested and compared to the 6 inch x 12 inch cylinders. The primary goal was provide additional data at a reduced size in order to allow using smaller models in the DEM simulations, hence decreasing runtimes. The stress-strain behavior of the repaired cylinder samples in splitting tension is shown in Figure 34 and the results are summarized in Table 6.

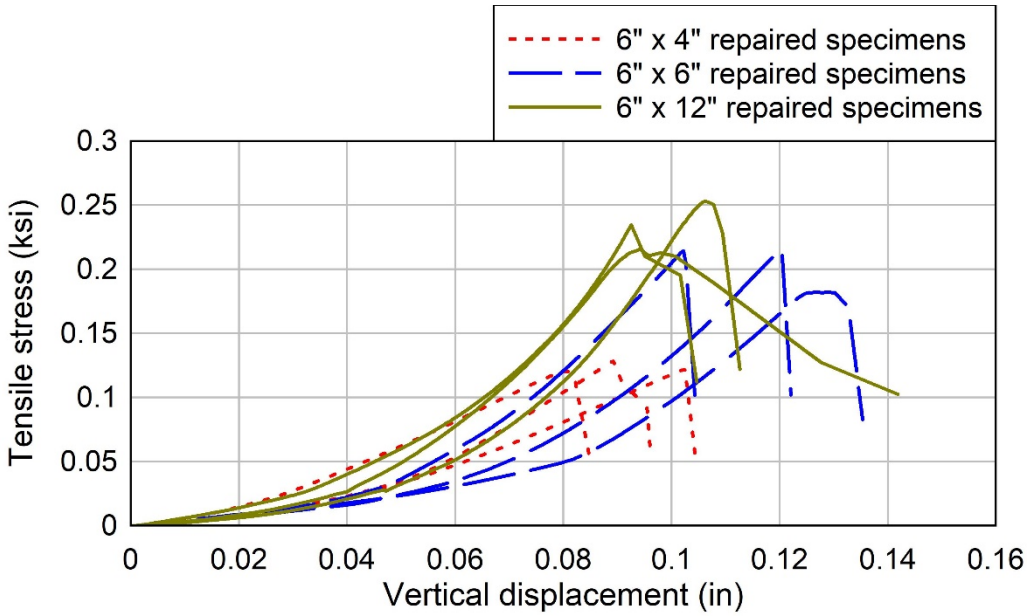

Figure 34:Splitting tension test results of epoxy repaired concrete cylinder specimens of various sizes.

Table 6: Summary of tensile strength of concrete cylinder specimen of various sizes.

Sample Size	***Average Tensile Strength (ksi)***
6 inch x 12 inch	0.23
6 inch x 6 inch	0.20
6 inch x 4 inch	0.13

CHAPTER 4. MORTAR CYLINDER EXPERIMENTS

4.1 Plain Mortar Experiments

As discussed in Section 1.2.2, the DEM models are tasked with characterizing fracture pattersn in plain concrete. The models require calibrating the mechanical parameters of particulate elements and bonds. The calibration is done in two steps: (i) calibration of the parameters of particulate elements and bonds in mortar; (ii) calibration of the parameters of particulate elements and bonds in aggregates and calibration of the parameters of the mortar/aggregate bonds. In order to fulfill objective (i), mortar cylinder tests were conducted. Similar to plain concrete, a series of tests were developed to evaluate the fracture behavior in the mortar subjected to both uniaxial compression and splitting tension loads. The DEM models were then validated by simulating the location and behavior of microcracks in the mortar matrix, coarse aggregate, and at the interface of the two throughout the duration of a tensile splitting experiment simulation.

4.1.1 Material

The mix design of the mortar was very similar to the mix design used in the plain concrete cylinder experiments. The mortar samples were made using the same ratio of water to cement (0.35) and the same ratio of fine aggregates to cement (1.5) as for the mortar matrix of the plain concrete samples. The mix design of mortar used is given in Table 7.

Table 7: Mortar mix properties.

Material	*Weight Fraction*
Cement	34.8%
Water	12.3%
Fine Aggregates	52.9%

The mortar was mixed by hand using the following steps:

1. The fine aggregate (sand) and cement were added to a large container
2. The sand and cement were fully mixed together using a mortar hoe
3. The water was added to mixture
4. The mortar mixture was fully combined using a mortar hoe
5. The mixture was poured into cylinder molds

4.1.2 Specimen

Two batches of mortar were produced. The first batch of mortar was made to determine the size effect of the mortar cylinders for specimen selection. Due to computational constraints, the model could only consider cylinders of 6 inch x 6 inch in tension. Sample sizes of 6 inch x 4 inch, 6 inch x 3 inch, and 6 inch x 2 inch are more computationally efficient. In order to ensure the most reliable tests, experiments were conducted to find the sample size that ensured the most consistent results. The following samples were cast and tested:

- Three 6 inch x 12 inch mortar in splitting tension
- Three 6 inch x 4 inch mortar in splitting tension
- Three 6 inch x 3 inch mortar in splitting tension
- Two 6 inch x 2 inch in splitting tension

The tensile stress-strain results of the splitting tension experiments for specimen of various sizes are shown in Figure 35. A summary of the average ultimate values as well as the coefficients of varitaion (COV) are given in Table 8.

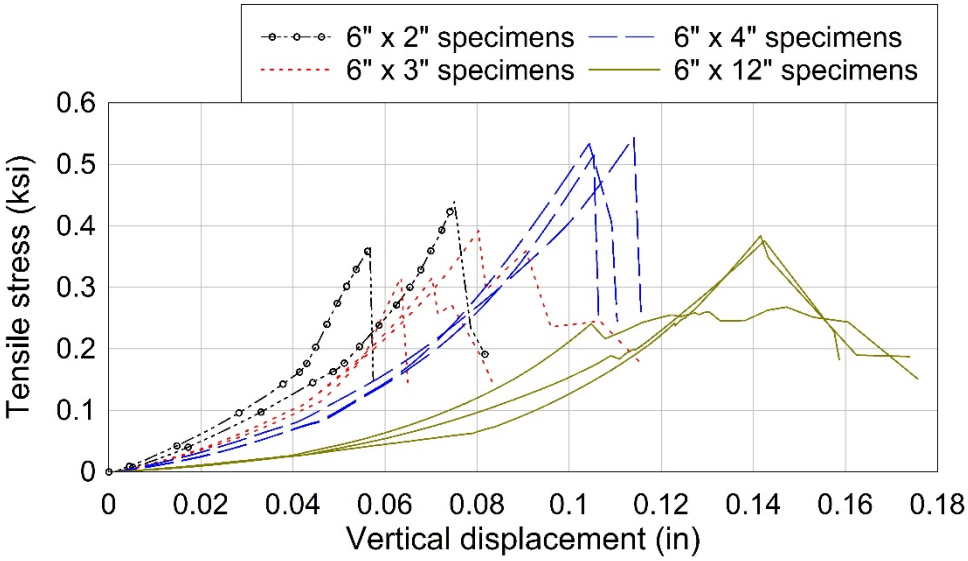

Figure 35: Splitting tension test results of mortar cylinder specimens of various sizes.

Table 8: Summary of average tensile strength and coefficient of variation of mortar specimen of various sizes.

Sample Size	***Average Tensile Strength (ksi)***	***Coefficient of Variation (COV)***
6 inch x 12 inch	0.351	18%
6 inch x 4 inch	0.558	3%
6 inch x 3 inch	0.376	12%
6 inch x 2 inch	0.455	N/A

The choice of which specimen size to use was judged based on the cofficient of variation (COV) of each size, consistency in failure mode, and average tensile strength. According to the literature, mortar alone should have a higher strength than the equivalent

concrete matrix with the same water to cement ratio (Hillerborg, 1985; Alexander and Mindess, 2005). The 6 inch x 4 inch samples were chosen as they had the lowest COV, provided the most consistent failure mode, and had a tensile strength greater than the concrete at 28 days. An example of the 6 inch x 4 inch typical breaking pattern is illustrated in Figure 36.

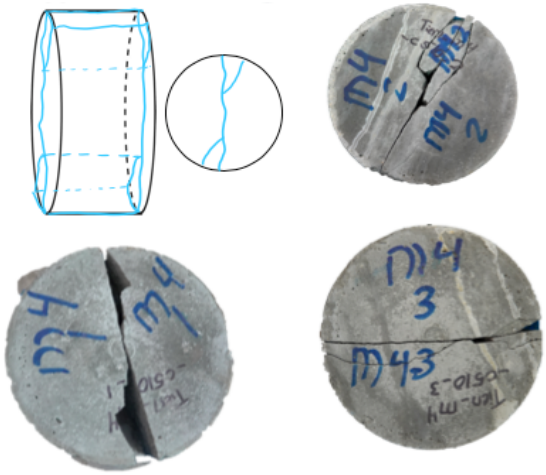

Figure 36: Typical failure patterns of a 6 inch x 4 inch mortar specimen.

4.1.3 Compression Experiments

A second batch of mortar using the same mix design and process was produced. This mixture was used to cast 6 inch x 4 inch mortar tension samples and 4 inch x 8 inch mortar compression samples. Results are presented in this section and the following.

The 4 inch x 8 inch mortar compression specimen were tested to find the uniaxial compression strength using a method based on ASTM C39. The compressive stress-strain behaviour for the three samples is shown in Figure 37. The average compressive strength of the mortar was 9.53 ksi. Consistent with the literature, the compressive strength of the mortar was found to be roughly twice that of the plain concrete at the same water content.

The mortar samples in compression exhibited a shear and columnar failure pattern as shown in Figure 38.

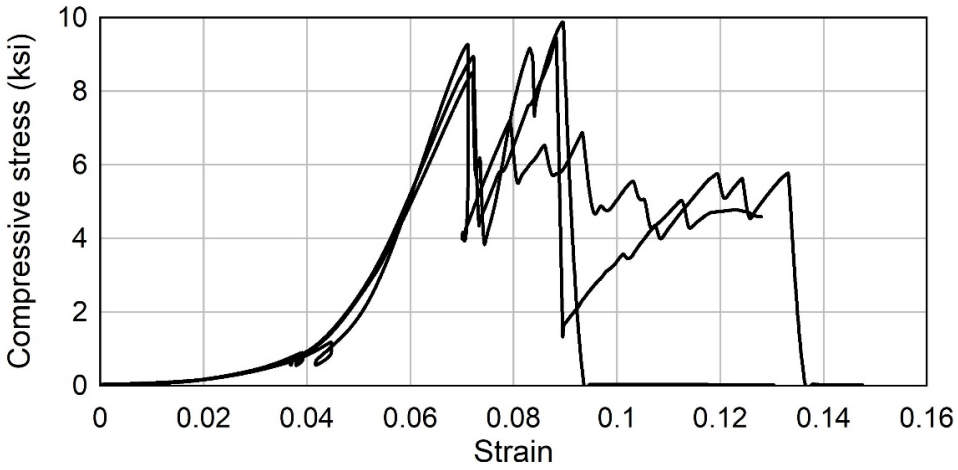

Figure 37: Compressive test results of mortar 4 inch x 8 inch cylinder specimens.

Figure 38: Typical failure pattern of mortar specimen.

4.1.4 Splitting Tension Experiments

The 6 inch x 4 inch mortar tension specimens made of the second batch were tested to determine the splitting tensile strength using a method based on ASTM C496. In addition to 6 inch x 4 inch samples, the three 4 inch x 8 inch mortar samples were tested to obtain

additional comparative data points for future research as the computer models are refined. The splitting tensile stress-strain curves are shown in Figure 39. Consistent with the literature (Alexander and Mindess, 2005; Mehta and Monteiro, 2006), the splitting tensile strength of the mortar (0.68 ksi) was found to be roughly twice that of the plain concrete (0.36 ksi) at the same water content. An example of the typical crack propagation of the 6 inch x 4 inch mortar sample is shown in Figure 40. The figure shows the specimen before any cracks develop, the onset of cracking near the midline, and the specimen at the ultimate tensile strength.

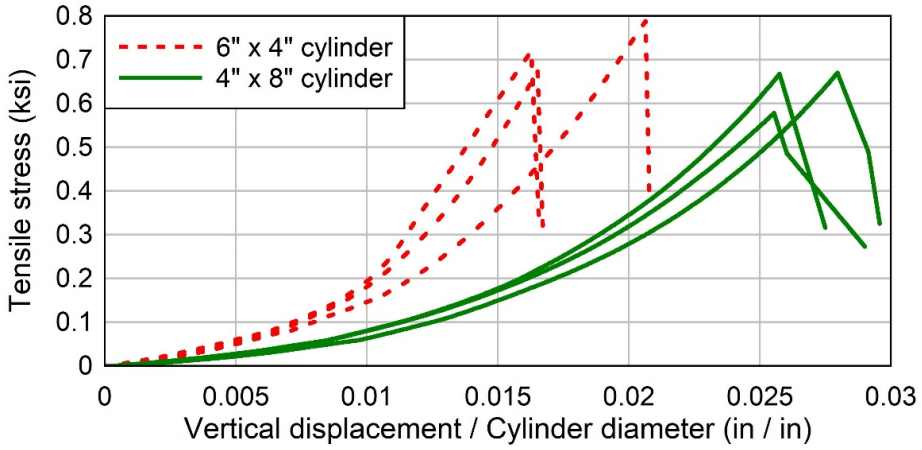

Figure 39: Splitting tension test results of mortar cylinder specimens of various sizes.

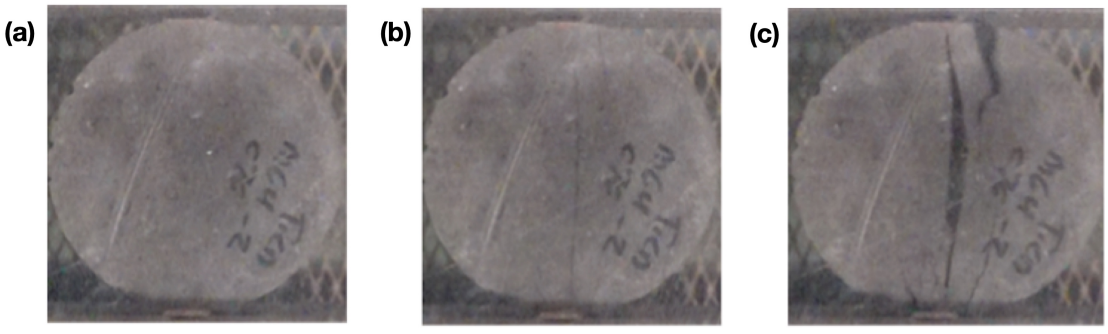

Figure 40: Behavior of mortar during splitting tension test: (a) before crack develops; (b) at onset of cracking; (c) at ultimate strength.

CHAPTER 5. BEAM EXPERIMENTS

The experiments presented in this chapter are divided into two categories: unreinforced concrete beam experiments (Section 5.1) and reinforced concrete beam experiments (Section 5.2). For both categories, experiments were conducted on "as-built" and epoxy-repaired concrete beams.

5.1 Unreinforced Beam Experiments

As discuessed in the literature review (Section 2.3.3), the unreinforced beams were designed to be experimentally characterized using Hillerborg's three-point bend test. To determine the flexural strength and fracture energy of the concrete, a specialized three-point bend test on a notched beam was used.

The unreinforced beams were cast using the same concrete that was used to produce the concrete cylinders discussed in Section 3.1.2. Since the three-point bend test is sensitive to the length of the beam, beams of both three-foot and four-foot lengths were cast using in-house wooden formworks, shown in Figure 41. Beams of both lengths had a cross-section of 6 inch x 10 inch. Drawings of the beams are included in Appendix A. Seventy-two hours after casting, the beams were demolded and placed in a controlled fog room environment for curing. At 56 days, the beams were removed from the controlled environment and allowed to age at ambient temperatures until their test date. As previously discussed in Chapter 3, plain concrete cylinder samples were tested in uniaxial compression and splitting tension each week throughout the duration of beam testing to quantify the compressive and tensile strength of the beam. The unreinforced beams were notched using a masonry saw to a notch depth of 3.25 inch, shown in Figure 42.

Figure 41: Concrete beam formwork.

Figure 42: Notching of concrete beams with masonry saw.

To achieve a “repaired” concrete state, the unreinforced beams of both 3 feet and 4 feet of length were cut completely into two halves and then reattached by the same HMWM

epoxy as the one used in the repaired concrete cylinders. The following describes the methodology used to prepare the unreinforced beam for repair with epoxy:

1. The unreinforced beam was cut into two halves with a masonry saw (Figure 43)

Figure 43: Preparation of epoxy-repaired beam: beam cut in half with masonry saw.

2. The notched region was prepared by inserting a single wall corrugated cardboard with thickness of 0.125 inch between the two halves (Figure 44a)
3. Construction silicon caulk was applied at the border of the repaired section on one half of the beam (Figure 44b)

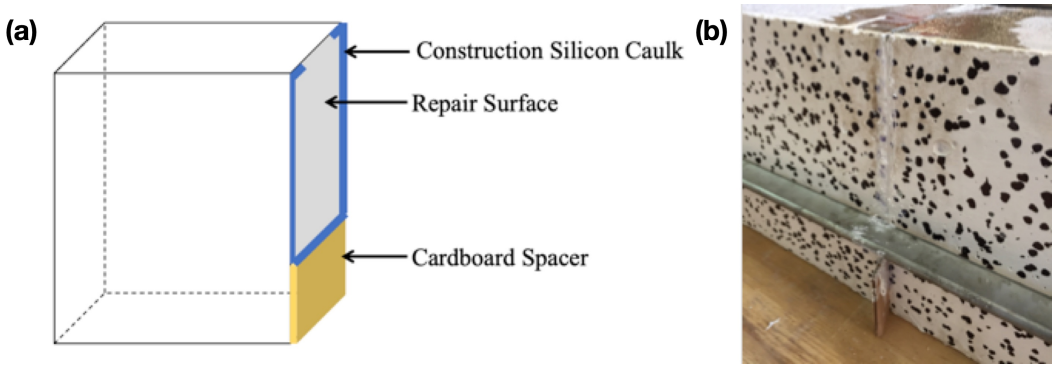

Figure 44: Preparation of epoxy-repaired beam: (a) diagram of silicon caulk and spacer placement; (b) silicon edging and cardboard spacer.

4. The two halves were compressed together, making sure they were aligned, and were tighten using long clamps (Figure 45)

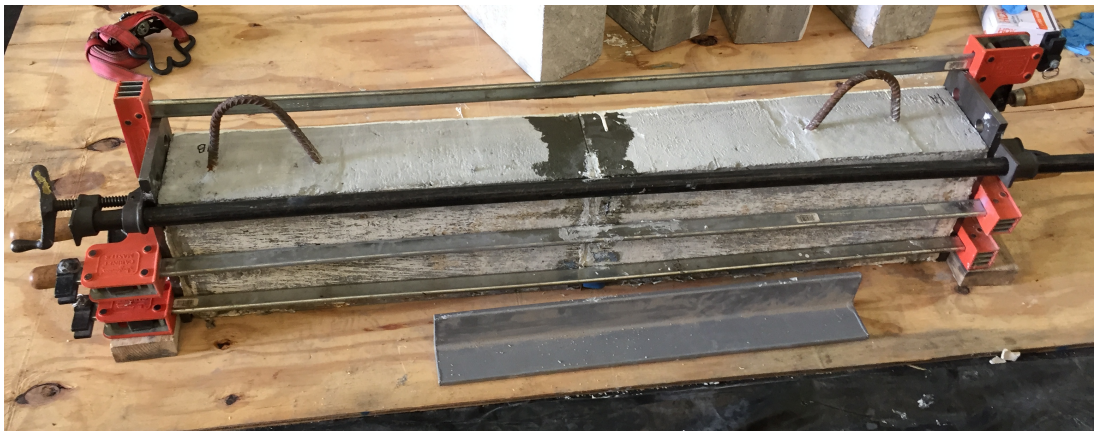

Figure 45: Preparation of epoxy-repaired beam: repaired beam clamped together for curing.

5. Any silicon that escaped the notch was smoothed out and more silicon was applied to securely seal the repaired section, if needed
6. The silicon was allowed to cure for at least 24 hours before applying epoxy

Once the silicon was cured, the HWMM was mixed. The epoxy was a three-part mixture using three ingredients with a 75 mL : 150 mL: 1 gal ratio of Cobalt Napthenate promoter, CHP initiator, and propietary Sealate Resin, respectively (Transpo Industries, 2017b). The epoxy was mixed with the same steps as with the epoxy-repaired cylinders, given in Section 3.2.1. The epoxy was then poured into the created "crack," shown in Figure 46a. Steel plates were used to guide the epoxy into the "crack" until it was completely full of the HWMM as shown in Figure 46b. After the crack was filled with epoxy, sponge paintbrushes were used to ensure the crack was completely filled with epoxy and level with the top of the beam. The epoxy was allowed to set for at least 48 hours.

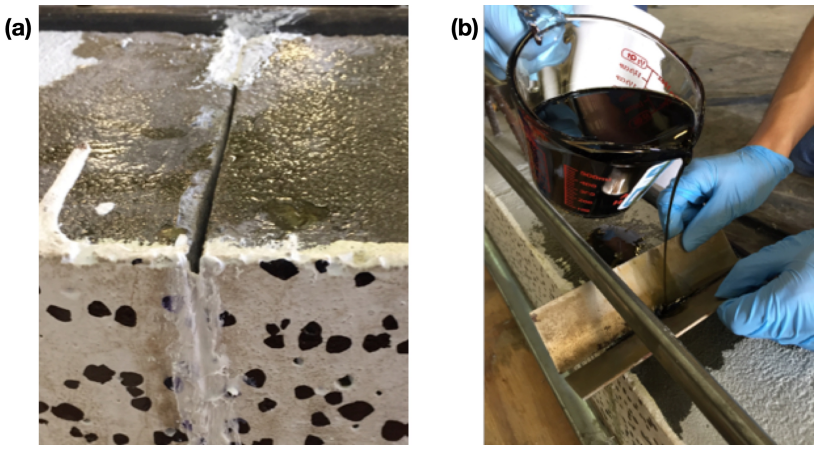

Figure 46: Preparation of epoxy-repaired beam: (a) "crack" opening of the repaired concrete beam; (b) pouring epoxy into "crack"

5.1.1 Experimental Setup

The setup of the three-point bend experiment is shown in Figure 47. A 50-kip, Interface 1220AO-50k load cell was connected to a Interpac hydraulic jack to apply a load at a rate of approximately 2 kips per minute. The notched unreinforced beams were set on roller supports to limit the effect of friction on the results. As the focus of these tests was to determine the fracture energy of the concrete, the two measurements of interest were global deflection and crack opening versus the load applied.

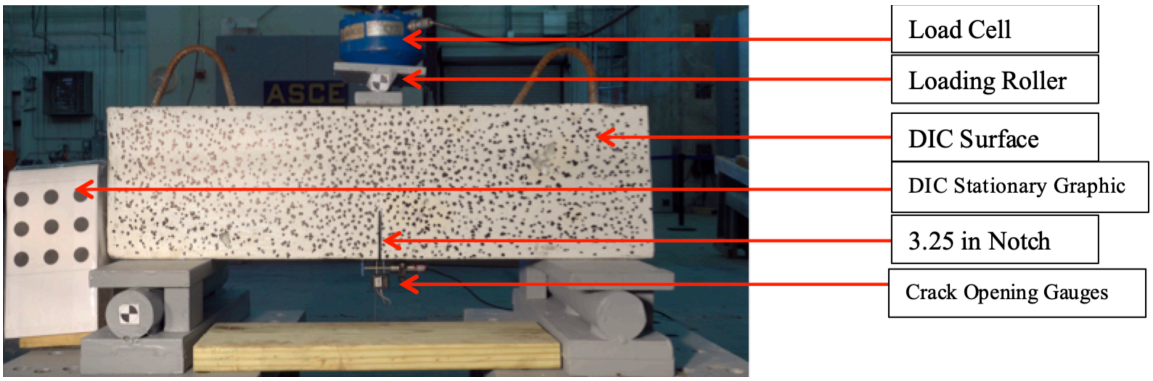

Figure 47: Three-point bend experimental setup.

To ensure redundancy in measuring the crack opening, two methods of measurement were used: a lateral variable differential transmitter (LVDT) and an extensometer. The RDP DCTH200AG LVDT used in this experiment had a maximum travel of +/- 0.2 inch. The extensometer used in this experiment was an MTS 6.3203E-20 clip-on extensometer with a maximum travel of 0.15 inch. Both measuring devices are shown in the photo in Figure 48.

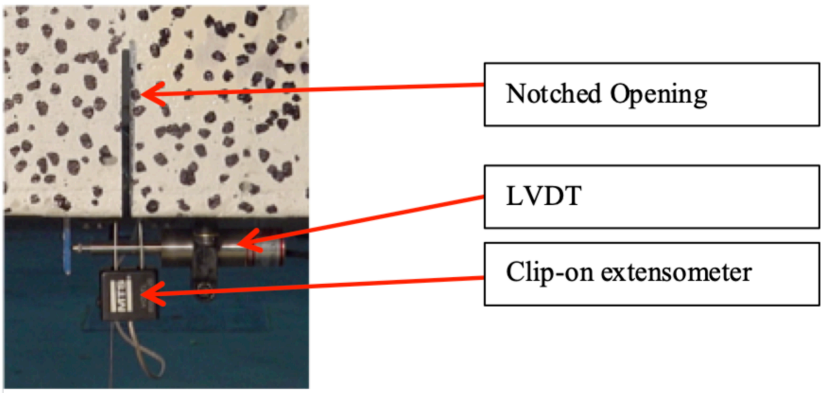

Figure 48: Crack opening instrumentation: LDVT and extensometer.

To ensure redundancy in measuring the global deflection of the beam, two methods of measurement were used: a stringpot gauge and digital image correlation (DIC). A Celesco PT1A-50-UP-500-M6_SG stringpot gauge was connected to a hook attached to the front face of the beam. This attachment is shown in Figure 49. The hook was connected to the beam using a small L-brace and fishing wire in order to prevent warping in the string pot.

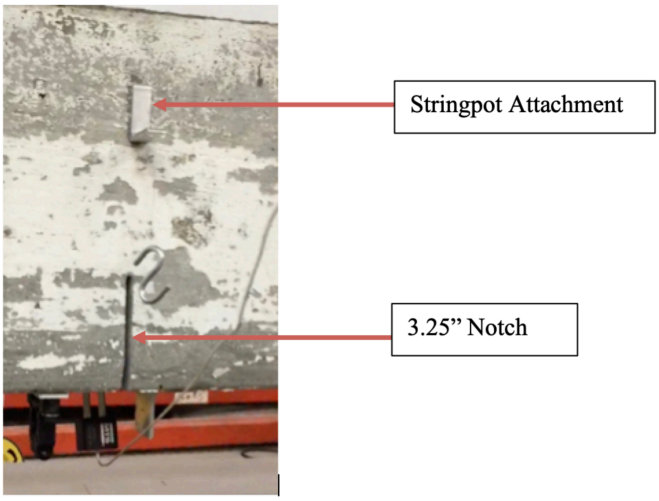

Figure 49: Deflection instrumentation: stringpot.

Digital Image Capture (DIC) was used to globally evaluate how the beam reacted to the applied load. A Sony RX10 Digital camera, which is capable of filming 1,000 fps over a four second duration was used to measure the beam, which had its entire front face painted white and marked with black dots for tracking. This treatment is referred to as a “DIC surface,” for simplicity. Although, the DIC system was not sensitive enough to measure the relatively small deflection of the unreinforced notched beams before total failure, it did provide valuable information about the beam’s global behavior. As a result, the stringpot was the main source of quantitative deflection data for the unreinforced notched beams.

5.1.2 Results

One of objectives of the three-point bend test was to find the fracture energy directly from the unreinforced notched beams. The crack mouth opening displacement was successfully captured by both the extensometer and the LVDT until the peak load. After peak load, the beams failed in a brittle maner within a short period of time, usually less than 1 second. As a result of this brittle failure and the associated sudden dramatic increase

of crack opening, the extensometer and LVDT typically detach from the beam. Therefore, the results were reliably captured until the peak load but not after the peak load.

5.1.2.1 Three-foot Beam Experiments

Five three-foot beams were successfully tested: three "as-built" specimen and two epoxy-repaired specimens. The applied load versus deflection behavior and the corrosponding crack opening displacement of the three-foot unreinforced notched beams are shown in Figure 50. In general, the epoxy-repaired beams performed better in terms of ultimate capacity than the intact concrete beams and also exhibited a slightly greater stiffness. An image of the typical failure of an "as-built" unreinforced notched three-foot beam can be seen in Figure 51 and the epoxy-repaired behavior can be seen in Figure 52. The epoxy-repaired concrete ehibited cracking within the concrete rather than along the interface.

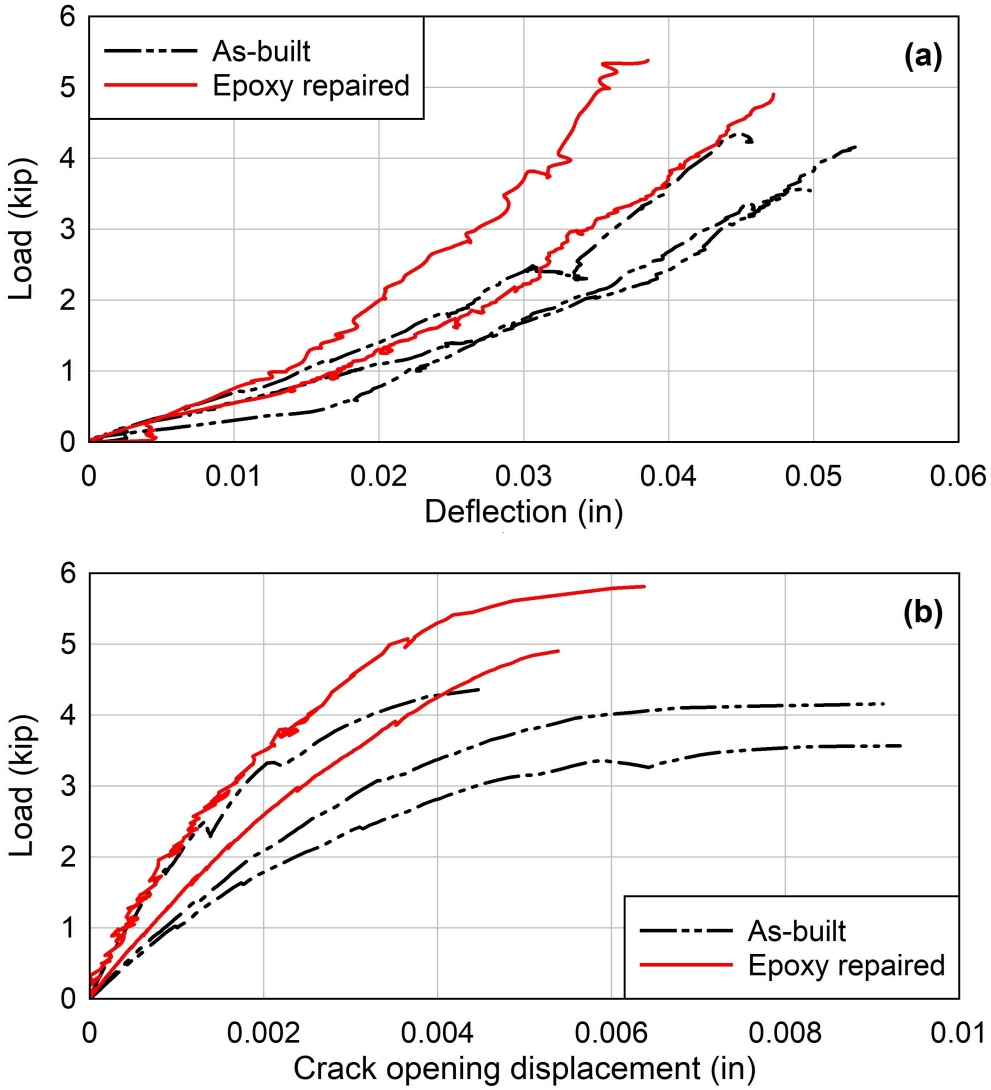

Figure 50: Test results of three-foot unreinforced concrete beams: (a) applied load versus vertical deflection at mid-span; (b) applied load versus crack opening displacement at mid-span.

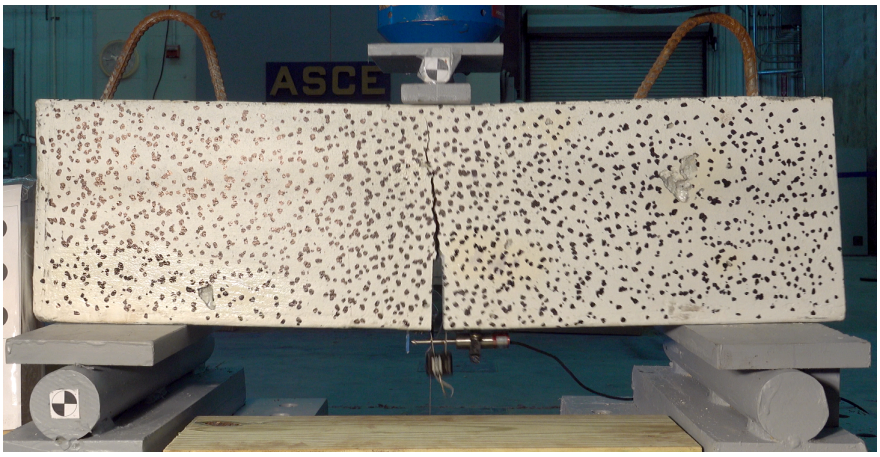

Figure 51: Three-foot "as-built" unreinforced concrete beam behavior.

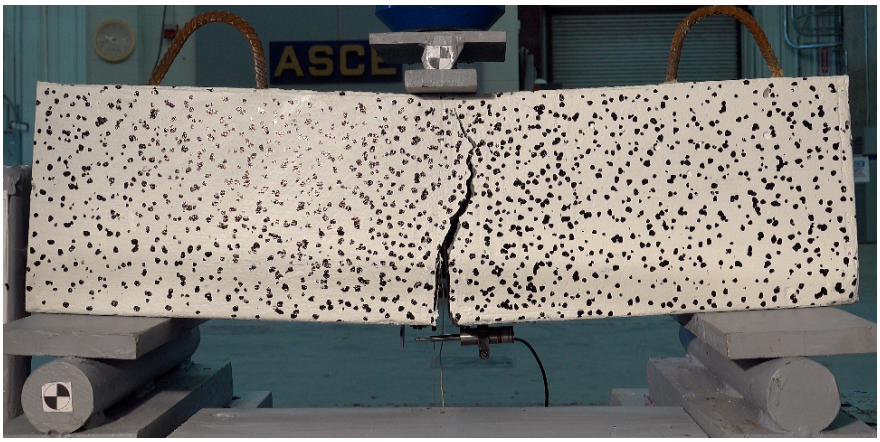

Figure 52: Three-foot epoxy-repaired unreinforced concrete beam behavior.

5.1.2.2 Four-foot Beam Experiments

After testing the three-foot beams, four four-foot beams were tested: two "as-built" specimen and two epoxy-repaired specimen. The experimental setup was altered to accommodate the larger beams by moving the location of the roller supports on the reaction frame. The load versus deflection curves and the corrosponding crack opening displacement of the four-foot unreinforced notched beams are shown in Figure 53. Similar to the three-foot beams, the epoxy-repaired beams, in general, performed better in terms of ultimate capacity than the "as-built" concrete beams. A photo of the typical failure of an

"as-built" unreinforced notched three-foot beam can be seen in Figure 54 and the epoxy-repaired behavior can be seen in Figure 55. The epoxy-repaired concrete ehibited cracking within the concrete rather than along the interface.

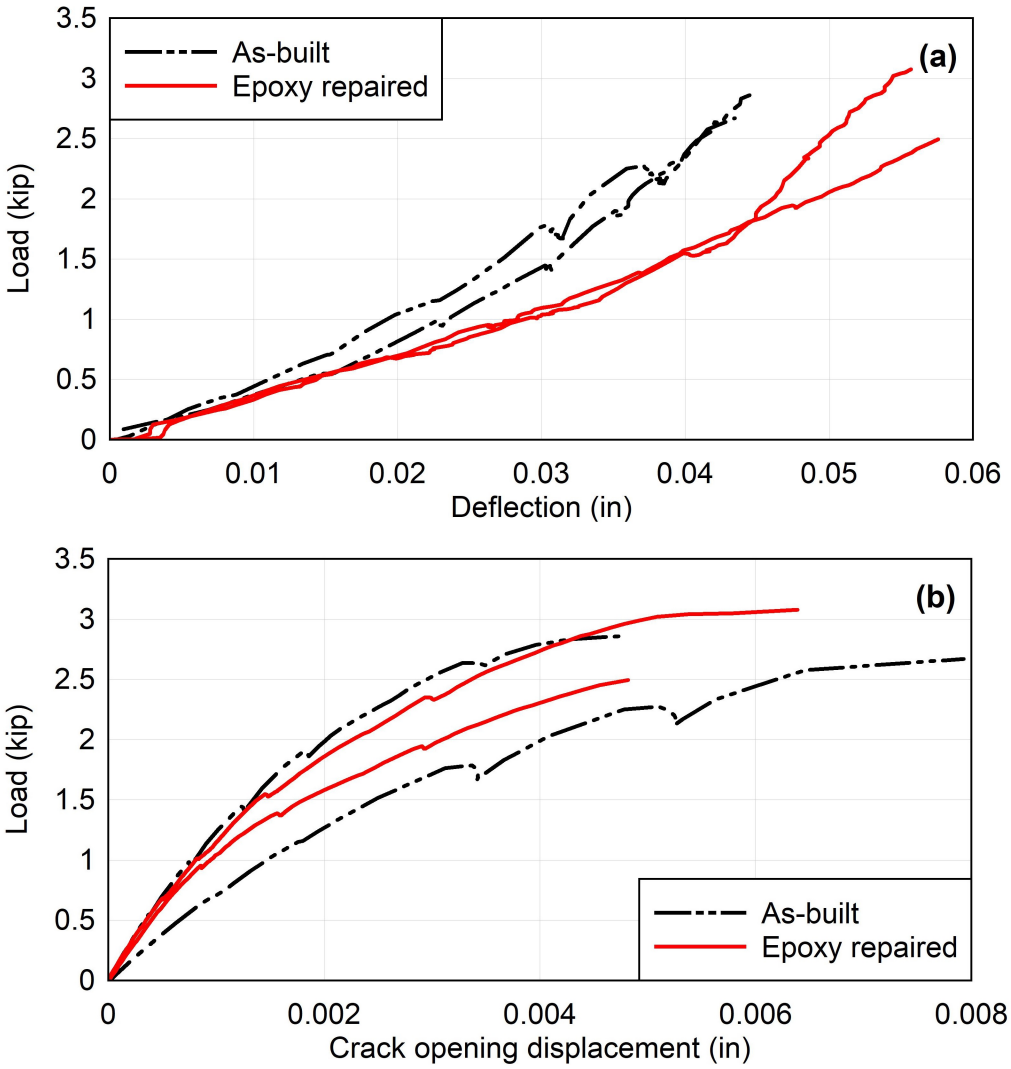

Figure 53: Test results of four-foot unreinforced concrete beams: (a) applied load versus vertical deflection at mid-span; (b) applied load versus crack opening displacement at mid-span.

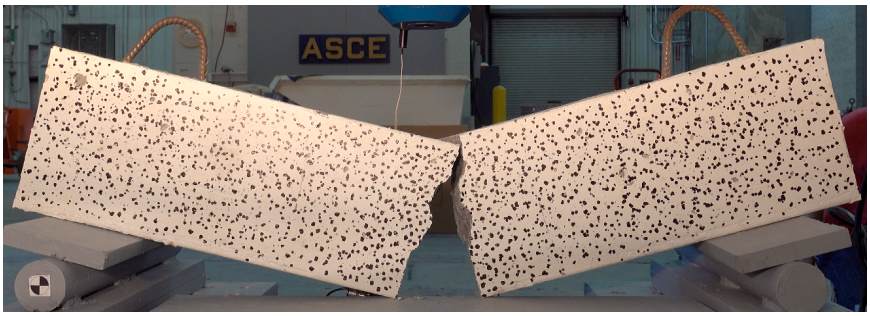

Figure 54: Four-foot "as-built" unreinforced concrete beam behavior.

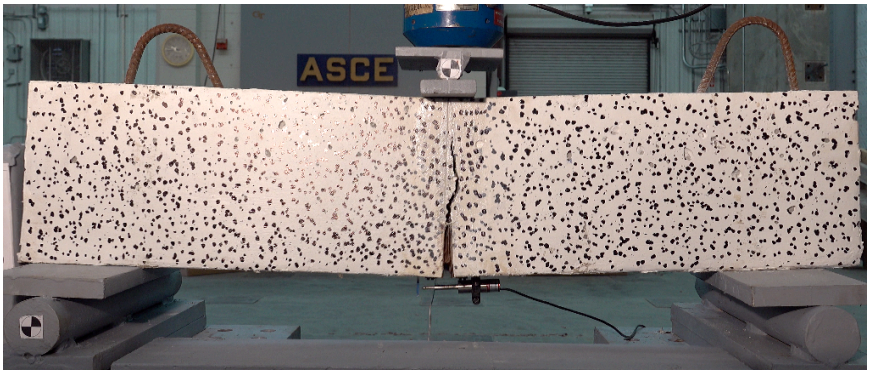

Figure 55: Four-foot epoxy-repaired unreinforced concrete beam behavior.

5.2 Reinforced Beam Experiments

The second beam type tested were reinforced concrete beams and included experiments of both "as-built" and epoxy-repaired specimen. In total, four reinforced concrete beams were tested. These beams were used to understand and quantify the effect of epoxy-repair of various size cracks on the beam's capacity with an application that is similar to that in the field.

5.2.1 Specimens

The beams were constructed in a manner similar to those described in Section 5.1.1, but these beams had the inclusion of reinforcing steel and no notch was cut. The beams

were cast on the same day as the notched beams and the concrete cylinders. Thus, the cylinder experiments of Chapter 3 can be used to quantify the material parameters of the beams. The beams were 4 feet in length and had a 6 inch x 10 inch cross section. The beams were longitudinally reinforced with two #6 rebars of 60 ksi steel. Structural drawings are located in Appendix A.

5.2.2 Experimental Setup & Procedure

The reinforced concrete beams used the same test setup as the unreinforced beams, except that crack monitoring gauges were not used because there was no notch. Instead, only the stringpot and DIC were used to measure the beam's deflection. The first experiment used a beam in its "as-built" configuration. The beam was tested to failure. The failure of the control beam is shown in Figure 56. This beam was used to observe the various crack sizes that were formed under different applied loadings (with associated displacements).

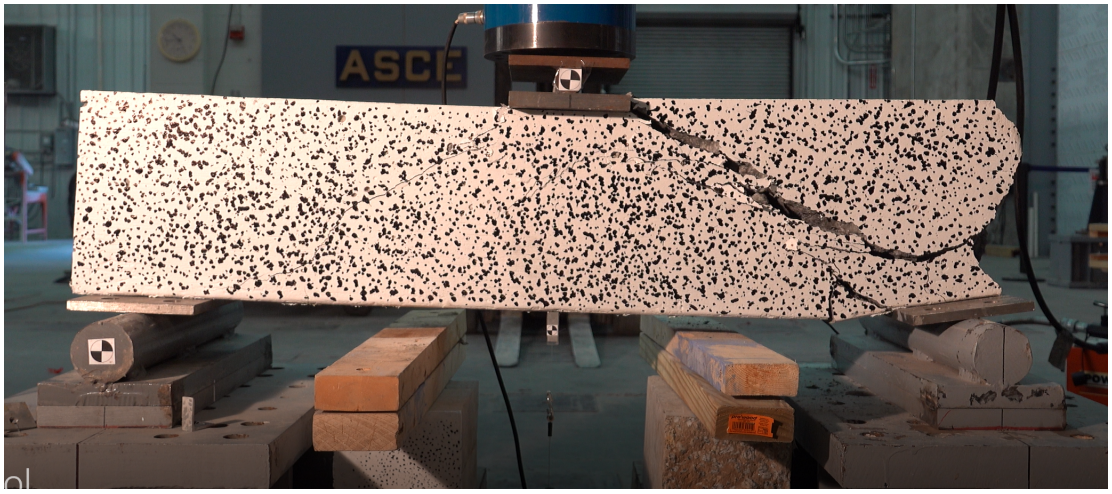

Figure 56: Behavior of "as-built" reinforced concrete beam at failure.

The remaining three reinforced concrete beams were loaded until minor hairline cracks (second beam) and major cracks (third and fourth beam) formed. Note that the

definition of “minor” and “major” cracks was internal to Georgia Tech and does not necessarily correspond to any internal GDOT definitions of crack sizes. Minor cracking, in this case, refers to cracks under the 0.006 in PCI minimum for epoxy injection. Major cracking refers to cracks at or above that limit. Once the cracks developed, the beams were unloaded and prepared for repair using the epoxy. The beams were removed from the frame and laid on their sides. The change in orientation of the beam allowed gravity to assist the epoxy flow as it filled the cracks. The epoxy and its preparation were the same as the previous concrete repair experiments. The epoxy was applied by coating the surface of the beams with the several layers of epoxy using a foam paintbrush. Once applied, the epoxy was allowed to cure for at least 48 hours before testing. Once fully cured, the beams were placed back on the testing frame and tested to failure using the same three-point bend test setup as the unreinforced four-foot beam experiments.

5.2.3 Results

The load versus deflection curve of the minor crack repair beam in comparison to the “as-built” beam is shown in Figure 57. The first peak shown on the graph represents the loading until the minor crack formed, as shown in Figure 58a. At this point, the beam was unloaded and repaired by epoxy. After the epoxy repair had finished curing, the beam was reloaded until the second peak occurred. Marked on the graph, this point represents the failure of the beam post-repair. This failure can be seen in Figure 58b. The repaired reinforced beam with minor cracking had a similar capacity to the “as-built” beam. In addition, the failure pattern of the repaired beam and the “as-built” beam were very similar. However, the minor crack repaired beam’s exhibited a more brittle behavior than that of the “as-built” beam, notably having a large reduction in capactity at about 25% of the ultimate strain of the “as-built” beam.

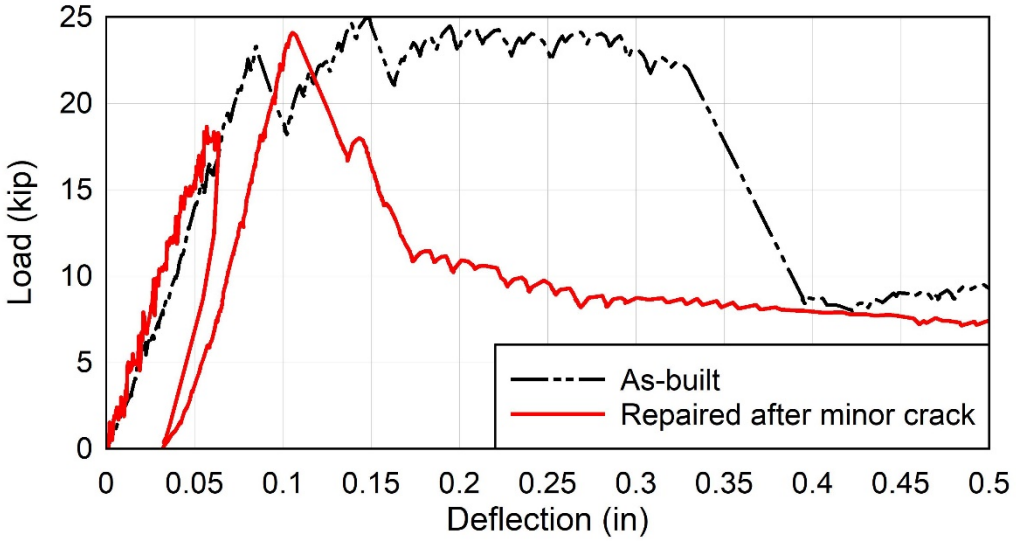

Figure 57: Load-deflection behavior of reinforced concrete beam repaired after minor cracks compared to as-built beam.

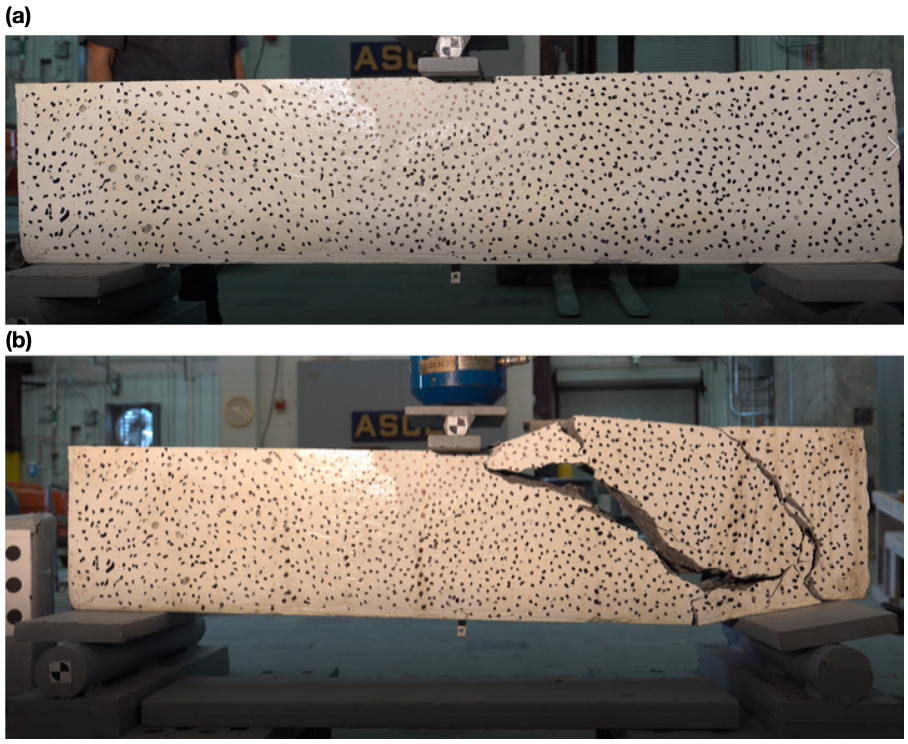

Figure 58: Behavior of reinforced concrete beam: (a) at minor crack development; (b) at failure.

The experiment was repeated on two beams that exhibited major cracks before repair. The load versus deflection behavior of the major crack repaired beams in

comparison to the “as-built” beam are shown in Figure 59. The first peak shown on the graph represents the loading until the major crack formed. The DIC analysis of this is shown in Figure 60a. As shown in the analysis, the major crack appears in the concentrated red section as the dots in this region had displaced the most from their original position. The second peak before complete failure represents the capacity of the beam after the epoxy repair. The DIC analysis of this event is shown in Figure 60b and a posttest photo is shown in Figure 61. In both cases, the beams repaired by epoxy after a major crack had developed was able to sustain approximately twice the load of the “as-built” beam. Interestingly, the failure strains of the beams were not the same and in one case, the failure strain was significantly less than the failure strain of the “as-built” beam.

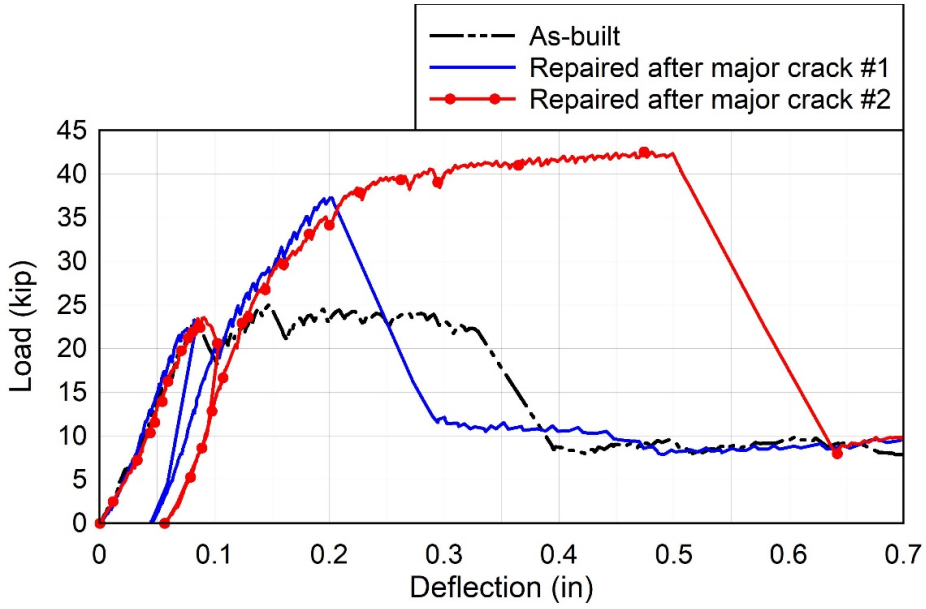

Figure 59: Load-deflection behavior of reinforced concrete beams repaired after major cracks compared to as-built beam.

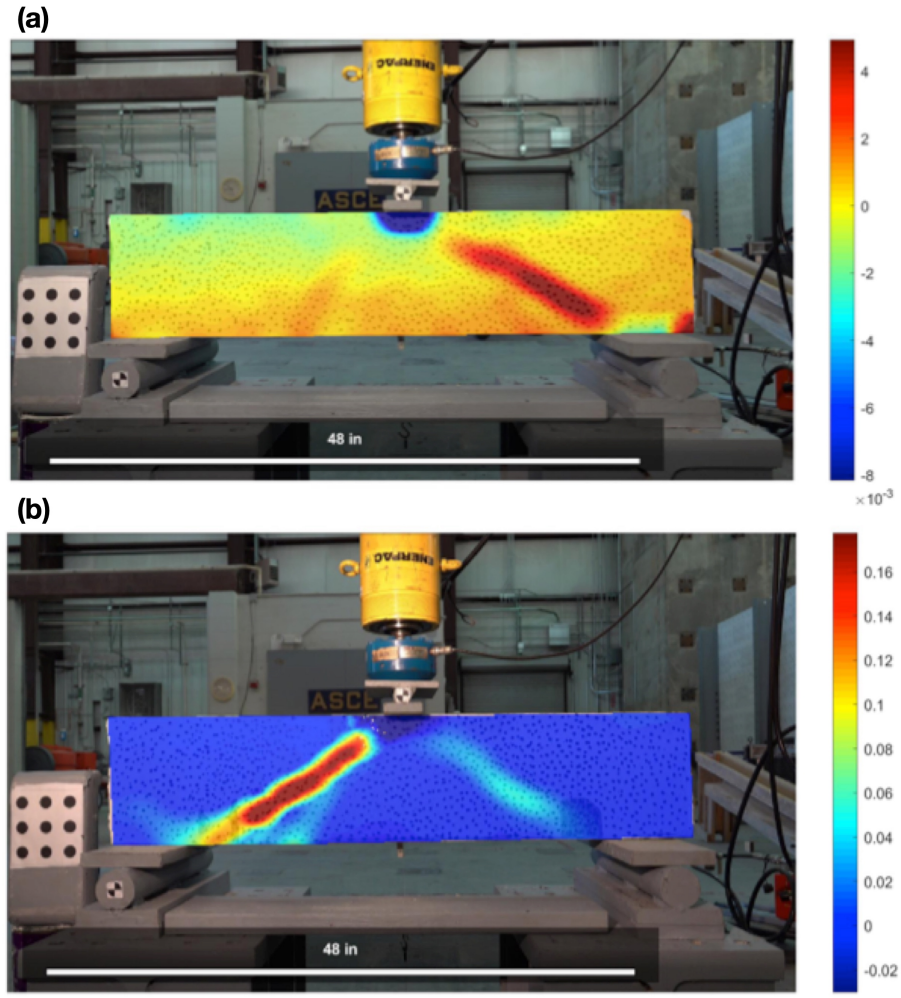

Figure 60: Behavior of epoxy-repaired reinforced concrete beam via DIC: (a) at major crack development; (b) at failure. Values in inches.

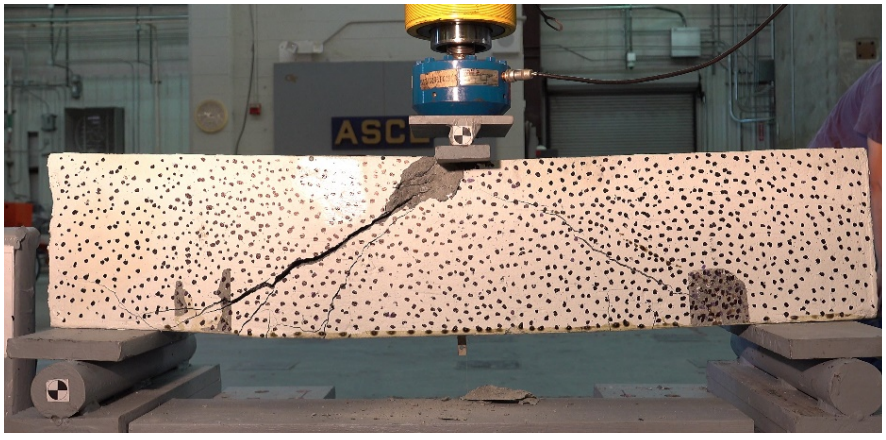

Figure 61: Behavior of epoxy-repaired reinforced concrete beam at failure.

The beams that were repaired after major cracks showed significant increases in capacity compared to both the as-built beam and the beam repaired after minor crack. One possible reason is that the relatively wider cracks on the beams loaded to major cracks allowed the epoxy to penetrate deeper into the beam. During the repair of beams after major cracks, visible epoxy droplets formed on the other side of the beams, indicating that the epoxy went through the whole section of the cracked beams. In contrast, this phenomenon was not observed during the repair of the beam after minor cracks, indicating that the relatively narrower cracks on the beam loaded to minor crack tended to prevent the epoxy from fully penetrating.

Another possible reason is that epoxy repair may change the force distribution inside the beam, and thus, the failure mechanisms and changed the overall capacity. As Figure 48 shows, major cracks appeared on the right hand side of the beam when initially loaded. After unloading and repairing, when loaded again, the beam failed with major cracks on the left hand side. This is possibly because the epoxy repairpenetrated into the right hand side of the beam through major crackes, which occurred during initial loading. This increased the strength of the local region on the right hand side. As a result, when the beam was loaded again, the left hand side was relatively weaker than the right hand side. Because of this difference in strength, the beam started to form new cracks at the left hand side instead of reopening the existing repaired cracks on the right hand side. The increase of ulitimate capacity may be related to the formation of new cracks on the left hand side of the beam.

CHAPTER 6. CONCLUSIONS

6.1 Summary and Conclusions

The research objective of this thesis was to develop and conduct experiments to measure the mechanical properties of cracked concrete repaired by epoxy in the laboratory in order to calibrate and validate the computational models created for the overarching research program. The main contribution of this research was the development and execution of an experimental method to characterize epoxy-repaired concrete by testing cylinders in uniaxial compression and splitting tension as well as a series of three point bend tests on both unreinforced and reinforced beams. The summaries of each individual chapter and the conclusions of the findings are included below.

Chapter 2 provided a literature review on the fracture mechanics of cracked concrete and crack propagation in concrete, effectiveness of epoxy repair in concrete, and an exploration of different experiments applicable to this research. The background research conducted lead to the development of the experimental testbed used to characterize the mechanical properties cracked concrete repaired by epoxy.

Chapter 3 described the experimental methods, specimens, and results of concrete cylinder experiments on both plain and epoxy-repaired specimens. The specimens were tested in both uniaxial compression and splitting tension. The methodology to create and test the epoxy-repaired cylinders called first for the cutting of plain concrete cylinders and repairing them using epoxy. The specimens were then to be tested using modified ASTM C39 and ASTM C496 procedures for uniaxial compression and splitting tension behavior to provide mechanical properties as well as qualitiative data (via high-speed cameras) to calibrate computational models. In comparison between the plain concrete and repaired

concrete, the plain concrete cylinders performed worse than the epoxy-repaired concrete cylinders in uniaxial compression. Although evidence from the qualitative data indicates that the epoxy repair may not have contributed to the higher ultimate compressive strength as an initial failure at the interface between the concrete and epoxy occurred well before the final fracture of the specimens. In comparison between the plain concrete and repaired concrete, the plain concrete cylinders performed better than the epoxy-repaired concrete cylinders in splitting tension. Evidence from the qualitative data indicates that the fracture of the specimen initiated at the interface between the concrete and the epoxy. In all, the development and excution of the new experimental method to create and test epoxy-repaired concrete created sufficient data to assist in the calibration and validation of the computational models.

Chapter 4 covered the experimental methodology, specimen details, and results of the mortar experiments. Uniaxial and splitting tension experiments were conducted on plain mortar cylindrical specimens in order to provide mechanical properties of the mortar as a separate material. In addition, studies on specimen size effect were conducted in order to determine the most computationally-efficient modeling scheme for the DEM model. In all, the mortar experiments successfully provided sufficient data to assist in the calibration and validation of the DEM computational model.

Chapter 5 contained the experimental methods, specimen details, and results of the beam experiments conducted on both “as-built” and epoxy-repaired specimens. Unreinforced concrete beam experiments were conducted on notched specimen. These tests included both plain concrete beams and beams that were repaired with an epoxy layer at a cut made directly above the notch. In all experiments involving the epoxy-repaired specimens, the crack initiated at the notch and then propagated through the concrete, away

from the interface. The epoxy-repaired specimen exhibited slightly higher ultimate strengths than the plain notched specimen. The research objective of developing a methodology to create comparable epoxy-repaired concrete specimens was successful as these experiments provided calidation data for the computational models. In addition to the unreinforced beams, five reinforced concrete beam experiments were conducted on "as-built" and epoxy-repaired specimen in order to provide simple validation data on the system level. The epoxy-repaired specimen were loaded to induce cracking of various levels, unloaded, repaired with epoxy, and reloaded to failure. In the cases where the cracks were very small (< 0.006 in), the epoxy did not have a significant effect on the ultimate capacity, but the beam behaved in a more brittle fashion. Interestingly, in the experiments where the cracks were larger (> 0.006 in), the beams exhibited a much higher capacity than the "as-built" ones. The failure mechanism and ductility of the beam were affected.

6.2 Recommendation for Future Work

The overall research was successful in developing an experimental testbed and methodology that provided the calibration and validation data for properly characterizing cracking behavior with and without epoxy for the computational models. However, three additions are recommended for future experimental approaches to allow for enhanced ways to test the computer models. These additions are: (1) improvement of repaired concrete methodology on cylinders; (2) utilizing alternative means to determine fracture energy; and (3) further testing on the recovered capacity of repaired reinforced concrete after a major (> 0.006 in) crack occurs.

6.2.1 Improved Repaired Concrete Cylinder Methodology

While the methodology for this research allowed for the collection of sufficient data for calibration, improvements to better control the epoxy dimensions and interface with the concrete should be implemented. The system used for this research was inconsistent, as it was difficult to apply a uniformly small layer of silicon to the cylinder that fully sealed the epoxy section. In addition, the hose clamps did not always provide adequate pressure to the cylinder to allow for a thin and uniform layer of epoxy to be applied. Moreover, the compressible nature of the cardboard spacer led to inconsistent epoxy thicknesses between specimens. The overall thickness and nonuniformity of the epoxy layer between the samples could be improved by implementing the following: the use of a rig to apply consistent uniform silicon caulk material to all cylinders, the use of a non-compressible spacers, instead of cardboard spacers, and the use of a superior clamping mechanism.

6.2.2 Alternative fracture energy techniques

Due to initial limitations in available lab equipment, the three-point bend test on notched beams was chosen to compute the fracture energy of the system. However, difficulties arose in this test during the softening regime due to the size effect and, more importantly, the data sampling rate. In future research, using an uniaxial tensile testing method or the wedge splitting test may better develop the softening curve of both the undamaged and repaired concrete.

6.2.3 Crack Development before Repair

A significant increase in capacity was observed in reinforced concrete beams that were repaired with epoxy after a major (> 0.006 in) crack had formed. This increased capacity was particularly interesting when compared to the lower capacity of beams that were repaired after only minor (< 0.006 in) crack development, as well as when compared

to beams that were uncracked. Because the repair significantly changed the overall behavior of the beam, it is recommended that additional research be conducted to understand the overall effect that using HWMM has on larger pre-stressed beams and, subsequently, the effect on the entire bridge structure including loads transferred to adjacent elements.

APPENDIX A. STRUCTUAL DRAWINGS

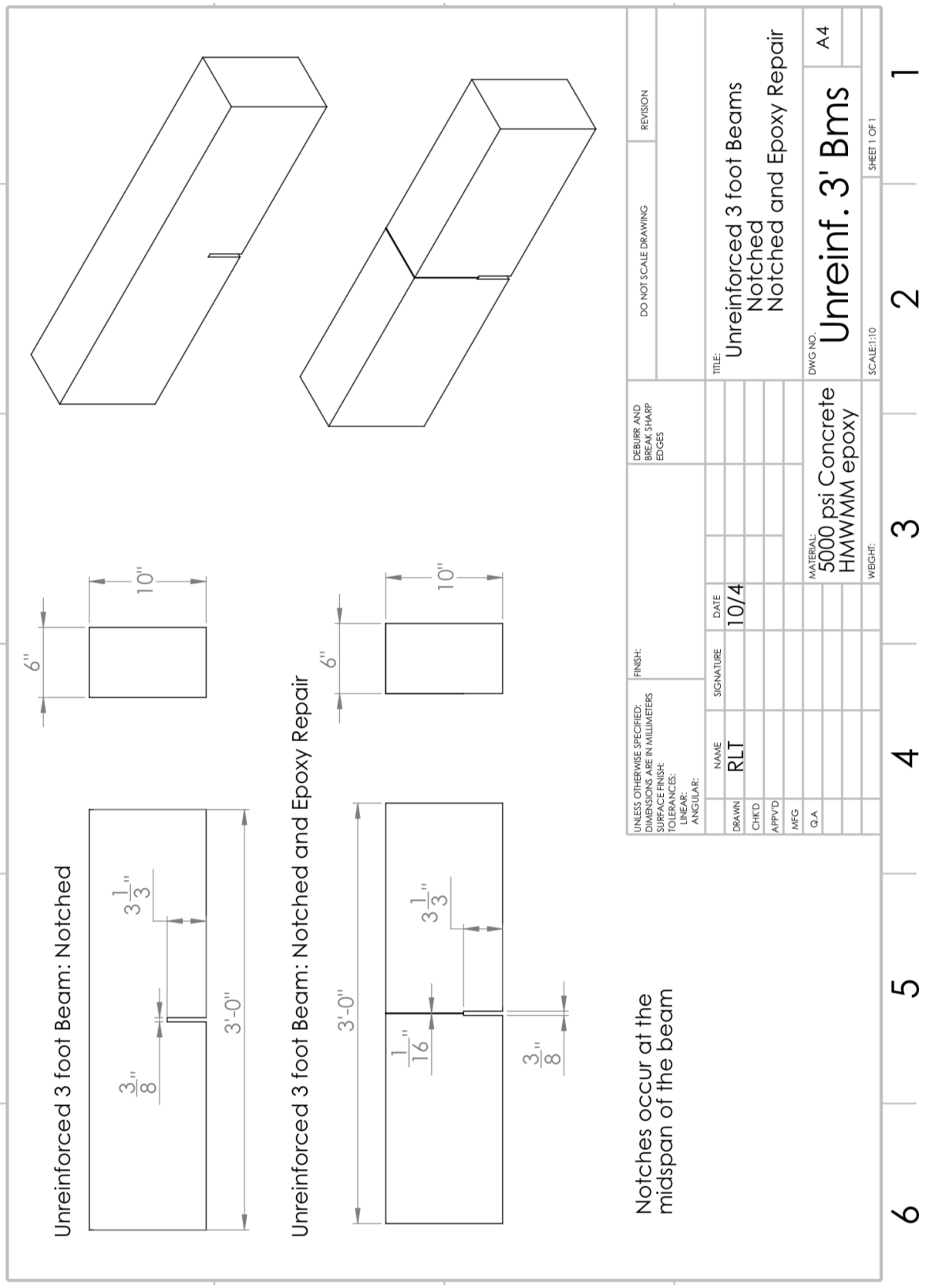

Unreinforced 4 foot Beam: Notched

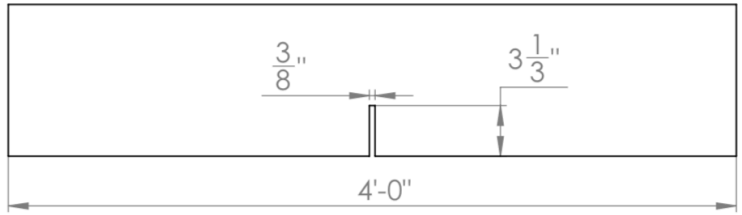

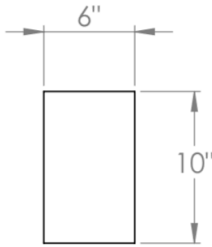

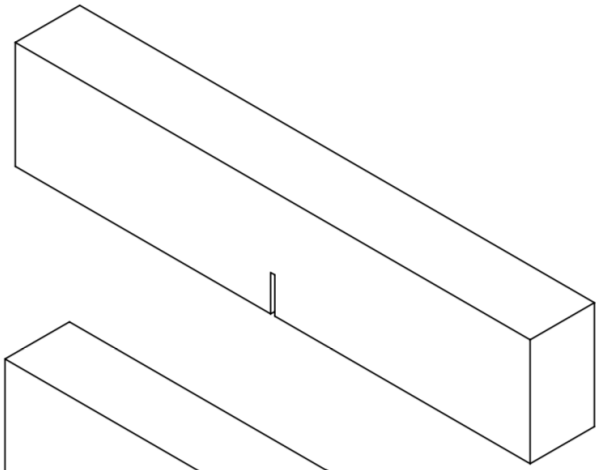

Unreinforced 4 foot Beam: Notched and Epoxy Repair

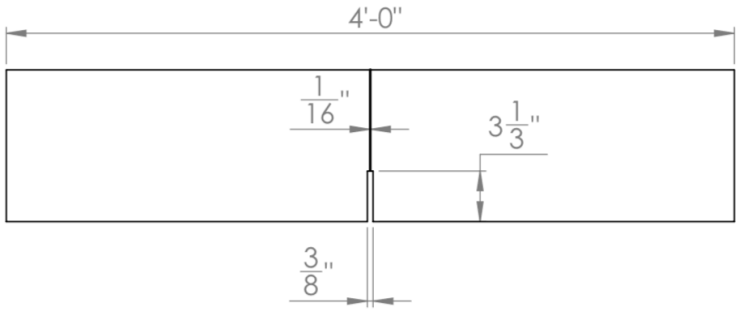

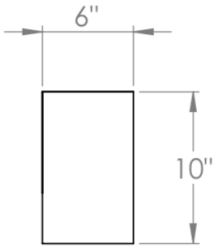

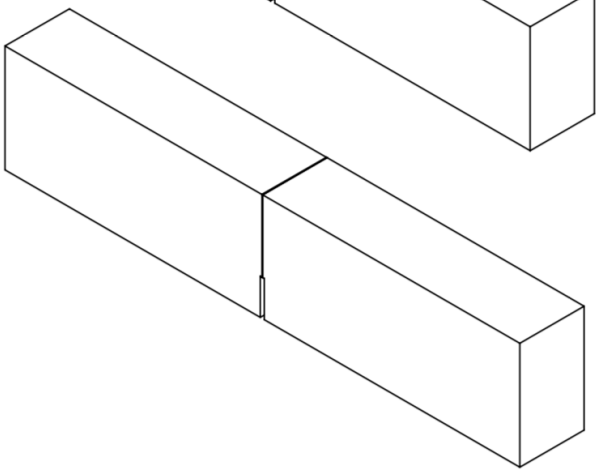

Notches occur at the midspan of the beam

UNLESS OTHERWISE SPECIFIED: DIMENSIONS ARE IN MILLIMETERS SURFACE FINISH: TOLERANCES: LINEAR: ANGULAR:		FINISH:		DEBURR AND BREAK SHARP EDGES		DO NOT SCALE DRAWING	REVISION
	NAME	SIGNATURE	DATE			TITLE: Unreinforced 4 foot Beams Notched Notched and Epoxy Repair	
DRAWN	RLT		10/4				
CHK'D							
APPV'D							
MFG							
Q.A				MATERIAL: 5000 psi Concrete HMWMM epoxy		DWG NO. Unreinf. 4' Bms	A4
				WEIGHT:		SCALE:1:10	SHEET 1 OF 2

Reinforced 4 foot Beam

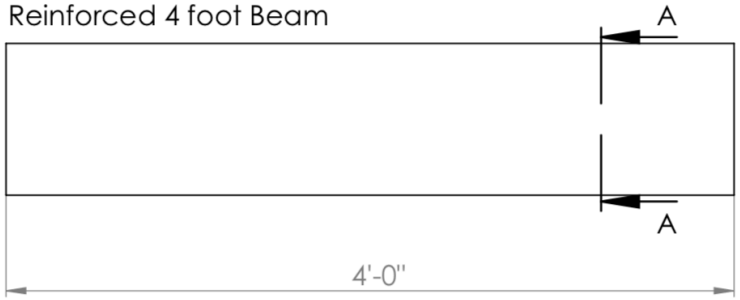

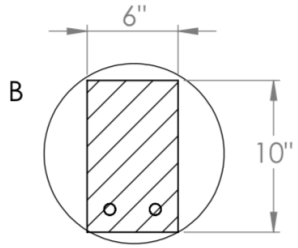

SECTION A-A

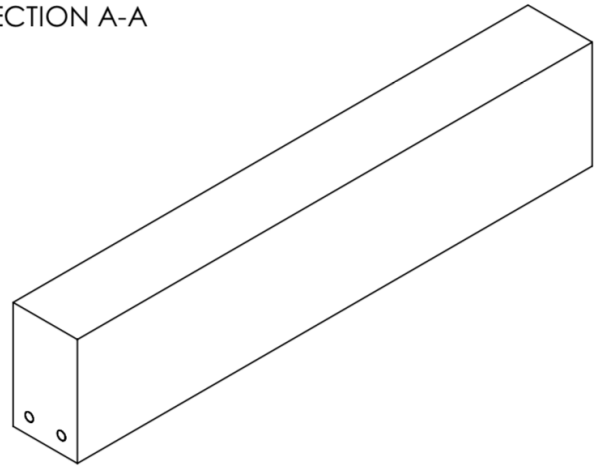

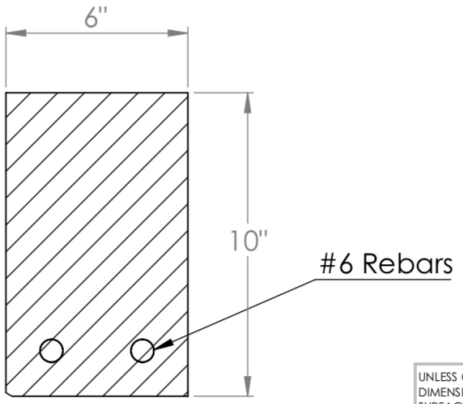

DETAIL B
SCALE 1 : 5

UNLESS OTHERWISE SPECIFIED: DIMENSIONS ARE IN MILLIMETERS SURFACE FINISH: TOLERANCES: LINEAR: ANGULAR:		FINISH:			DEBURR AND BREAK SHARP EDGES	DO NOT SCALE DRAWING	REVISION
	NAME	SIGNATURE	DATE			TITLE:	
DRAWN	RLT		10/4			Reinforced 4 foot Beams	
CHK'D							
APPV'D							
MFG							
Q.A				MATERIAL: 5000 psi Concrete HMWMM epoxy		DWG NO. Reinf. 4' Beams	A4
				WEIGHT:		SCALE:1:10	SHEET 1 OF 1

APPENDIX B. THOMAS CONCRETE MIXTURE

Thomas_Concrete,_Inc.
2500_Cumberland_Pky_S-200
Atlanta, Georgia 30339

DEPARTMENT OF TRANSPORTATION - HIGHWAY DIVISION
PORTLAND CEMENT CONCRETE MIX DESIGNS

Date: 3-16-18

CONCRETE PLANT: 737

PLANT LOCATION: Atlanta

MATERIALS		CODE	TYPE	SPGR	%ABS	F/F
Cement:	Holcim US, Inc. Holly Hill, SC	22	1	3.14		
Cement:	National Cement Co. of AL, Inc. Ragland,AL	41	1	3.14		
Sand Primary:	Vulcan Materials Co. Norcross,GA (10SM)	107F	2	2.69	0.30	
Stone:	Vulcan Materials Co. Norcross,GA	048	2	2.71	0.48	
Admixture:	Sika Corporation Plastiment Type D Lyndhurst,NJ.	14	1			
AEA:	Sika Corporation "SIKA AEA-14"					

CHECK MIX USED

ONE CUBIC YARD PROPORTIONS (SSD)

Class Concrete	24 HR ACCEL.	ONLY FOR USE ON DOT PROJECTS FOR EMERGENCY ROAD REPAIRS 1/11/2017						
Cement (lbs.)	752							
Sand -Primary (lbs.)	1045							
Stone (lbs.)	1893							
Water (gals.)	35.0							
Design Air (%)	4.0							
Accept. Air (LL-UL)	3.0 - 6.0							
Water Reducer (ozs.)	*- *							
Retarder (ozs.)	*- *							
Fine Agg Ratio (F/A)	0.36							
Stone Size	57							
Design Slump (ins.)	3.00							
Accept. Slump (LL-UL)	2.0 - 5.0							
Max. Water/Cu.Yd.	40.6							

737-4.1

LL=Lower Limit; UL=Upper Limit

* Retarder will be used when required by Specifications or placement conditions dictate it.

. Refer to temperature/dosage chart for retarder dosages.

The above concrete mix design proportions are for use on Department of Transportation projects. The ability of these proportions to produce concrete that meets specification requirements remains the responsibility of the Contractor. Jobsite acceptance of concrete produced with these proportions shall be based upon the Standard Specifications and SOP-10.

Concrete Engineer
or Certified Technician Jeff Duckworth

01/2017

Plant	: Atlanta		
Start Time	: 03/16/18 09:43:51	End Time	: 03/16/18 09:44:50
Product Code	: 508000	Destination	: Loadout
Load Size	: 3.00	Ticket	: 7365326
Truck No.	: 2742	Load Id	: 72010
Job	: 221	Customer	: GEORGIA TECH
Water Trim	: -2 gal	Moist. Water	: 18.99
Ideal W/C	: 0.3773	Acutal W/C	: 0.3545

MATERIAL	DESIGN	TARGET		ACTUAL		MST	ABS
TYPE I	752.00	2256.00	lb	2260.00	lb		
57 STONE	1858.00	5574.00	lb	5800.00	lb	0.00%	0.00%
MANUFACTURED SAN	1061.00	3336.74	lb	3440.00	lb	4.83%	0.00%
WATER	34.00	77.58	gal	77.00	gal		
AIR 14	7.20	21.60	floz	21.00	floz		
PLASTIMENT	11.30	33.90	floz	34.00	floz		

SCALE	START TARE	END TARE
AggLoadCell1	0 lb	5820 lb
AggLoadCell5	0 lb	3440 lb
CemLoadCell1	15 lb	2275 lb
WtrLoadCell1	0 gal	77 gal

APPENDIX C. TRANSPO INDUSTRIES SEALATE T-70

CASTEK® INC.
A TRANSPO INDUSTRIES COMPANY

Technical Data Sheet

High Molecular Weight Methacrylate (HMWM) Crack Sealer
Sealate® (T-70-10 and T-70 MX-30)

Sealate® is a specially formulated, high molecular weight methacrylate resin system that is highly effective for sealing and filling cracks in concrete structures.

Application Procedure

Surface Preparation: It is strongly recommended that all concrete surfaces that are to receive Sealate® be thoroughly clean and sound. Remove all surface dirt, grease, paint, rust, and other contaminates by sand blasting or shot blasting. Applications on LMC overlays do not require blasting or mechanical abrasion, the surface can be high pressure washed to remove contamination. Before application of Sealate® the surface must be dry for 24 hours and just prior to application cracks should be cleaned with dry high pressure compressed air. The concrete surface should be visibly dry and the moisture content in the concrete should be tested according to ASTM D4263. The ambient temperature should be between 50ºF and 100ºF prior to resin application.

Mixing: Table 1 lists the mixing ratios of the two curing agents. Add the appropriate amount of Cobalt Napthenate promoter to Sealate® resin and mix well. Then add the corresponding amount of CHP initiator, stir again for approximately one to two minutes. If mechanically applied, the resin should be mixed utilizing a two component resin system using promoted resin for one part and initiated resin for the other part. Mixing ratio of promoted/initiated resin should be 1:1. The mixed resin should be applied to the concrete surface within five minutes of complete mixing.

Table 1: Mixing Instructions for Sealate®, Cobalt Napthenate and CHP

Sealate® (gal)	Cobalt Napthenate (mL)	CHP (mL)
1	75	150
5	375	750

CAUTION: Never mix CHP initiator with Cobalt promoter. A violent reaction will result!

Application: The rate of application of mixed resin should be approximately 100-150 square feet per gallon. However, this will vary depending on the surface, porosity, size, and quantity of cracks present in the area being treated.

During application, the concrete surface should be flooded with the resin, allowing sufficient time for penetration into the surface and complete filling of all cracks. Excess material should be redistributed using squeegees or brooms within 15 minutes after application. The quantity of initiated/promoted resin mixed at one time should be limited to five gallons.

Broadcasting of Aggregate: Broadcast sand should be applied to the entire treated area prior to cure, typically at 1-2 pounds per square yard. The sand used should be 12 x 16 mesh, #1 or #2 blasting sand, and should have a maximum moisture content no greater than 0.5%. It should be placed within 15 minutes of the resin application and before any setting of monomer occurs. Traffic can be restored once the concrete surface is cured tack-free. Refer to Table 2 for temperature restrictions and cure times.

Table 2: Cure Times for Sealate®

Ambient Temperature	Approximate Cure Time	
	T-70-10	T-70 MX-30
50°F – 70°F	7 – 12 hr	8 – 16 hr
70°F – 100°F	4 – 7 hr	5 – 8 hr

*Cure times are approximate and will vary with ambient and deck temperature, humidity, and sunlight. Structures can be opened to traffic only after complete cure is achieved.

TRANSPO
The Smart Solutions Company

ISO 9001 REGISTERED FIRM

Table 3: Properties* of Sealate®

Property	Results		Test Method
	T-70-10	T-70 MX-30	
Viscosity	15 – 25 cps (MPa-sec)	10 – 25 cps (MPa-sec)	ASTM D2395
Density	8.6 lb/gal (1.03 g/mL)	8.5 lb/gal (1.02 g/mL)	ASTM D1425
Gel Time/Pot Life @ 70ºF	35 – 40 min	50 – 60 min	AASHTO T237
Tack Free Time @ 70ºF	4 – 7 hr	5 – 8 hr	AASHTO T237
Solids Content	100%	100%	ASTM D1644
Tensile Strength	1,600 psi (>11.0 MPa)	>1,100 psi (>7.6 MPa)	ASTM D638 Type I
PCC-SSD Bond Strength	>615 psi (>4.2 MPa)	>615 psi (>4.2 MPa)	CA Test 551
Tensile Elongation	1 – 5%	>30%	ASTM D638 Type I
Volatile Content	30% max	40 – 45%	ASTM D2369
Slant Shear Bond Strength	>2,000 psi (>13.8 MPa)	>2,000 psi (>13.8 MPa)	ASTM C882
Vapor Pressure @ 77°F	0.62 mm Hg	0.52 mm Hg	ASTM D323 Reid Method

*To be used as general guidelines only

Packaging

Sealate® comes in one, five and fifty-five gallon containers. The initiator, Cumene Hydroperoxide (CHP) and the Cobalt Napthenate promoter are provided in separate labeled containers and in pre-measured quantities to make scale mixes of Sealate®.

Storage

Sealate® should be stored in tightly sealed containers in a dry location and at normal room temperatures (50ºF - 85ºF). The initiator, Cumene Hydroperoxide (CHP) and the Cobalt Napthenate promoter are provided in separate labeled containers, and should be stored in a cool shaded area separately from each other as well as away from the monomer.

Caution

Direct contact with Sealate® may produce minor skin irritations to persons prone to such reactions. It is recommended that all persons involved in mixing and application wear protective clothing such as goggles, rubber boots, and rubber gloves. As with all chemicals, read SDS prior to use.

Warranty

The following warranty is made in lieu of all other warranties, either expressed or implied. This product is manufactured of selected raw materials by skilled technicians. Neither seller nor manufacturer has any knowledge or control concerning the purchaser's use of product and no warranty is made as to the results of any use. The only obligation of either seller or manufacturer shall be to replace any quantity of this product that proves to be defective. Neither seller nor manufacturer assumes any liability for injury, loss or damage resulting from use of this product.

20 Jones Street, New Rochelle, NY 10801

Tel: 914-636-1000
Fax: 914-636-1282
Web: http://www.transpo.com
Email: info@transpo.com

APPENDIX D. ADDITIONAL DATA

D.1 Three Foot Unreinforced Load vs Crack Opening

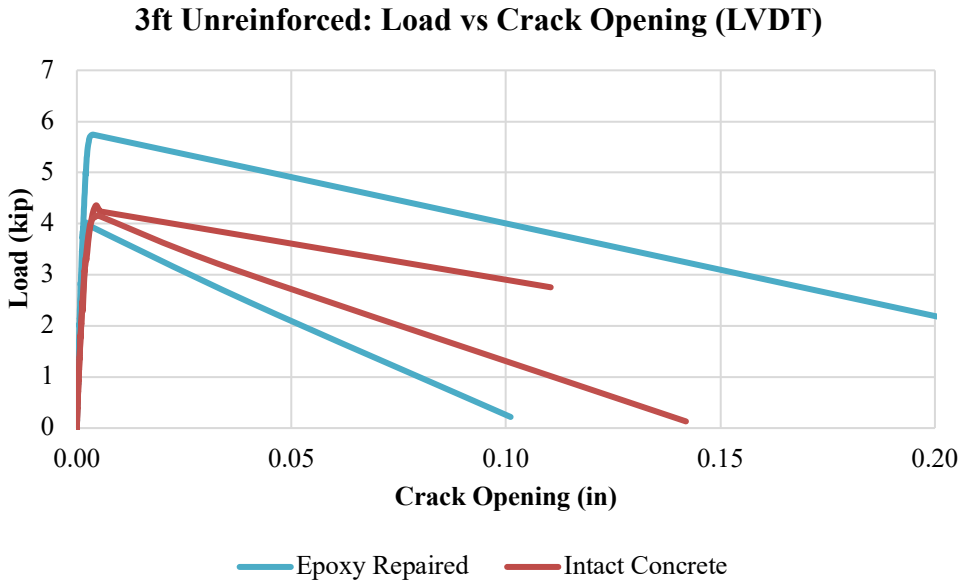

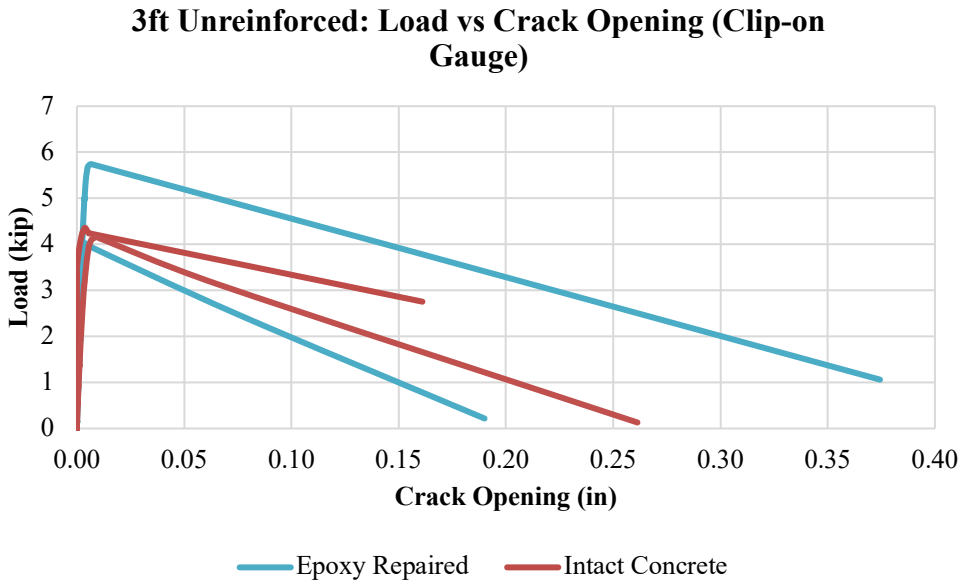

D.2 Four Foot Unreinforced Load vs Crack Opening

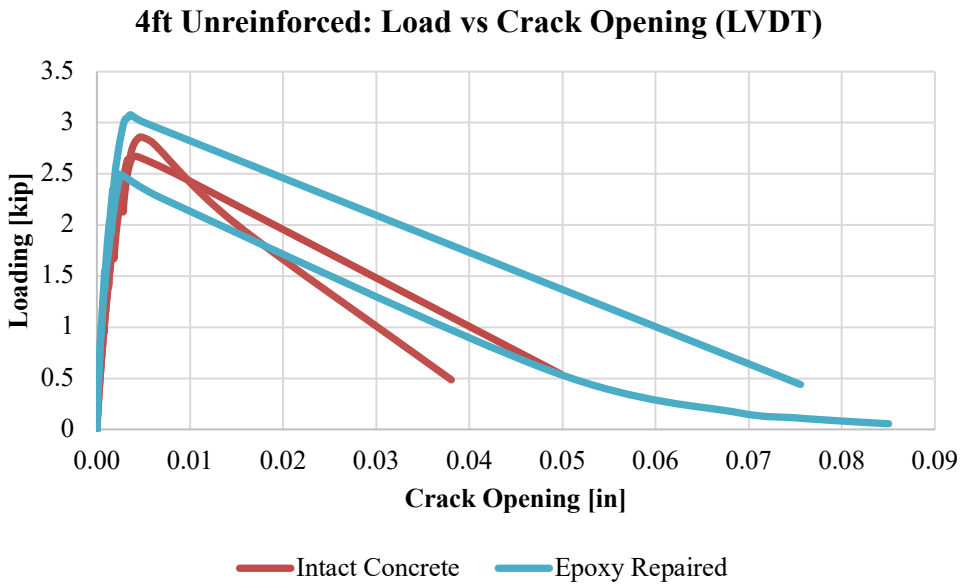

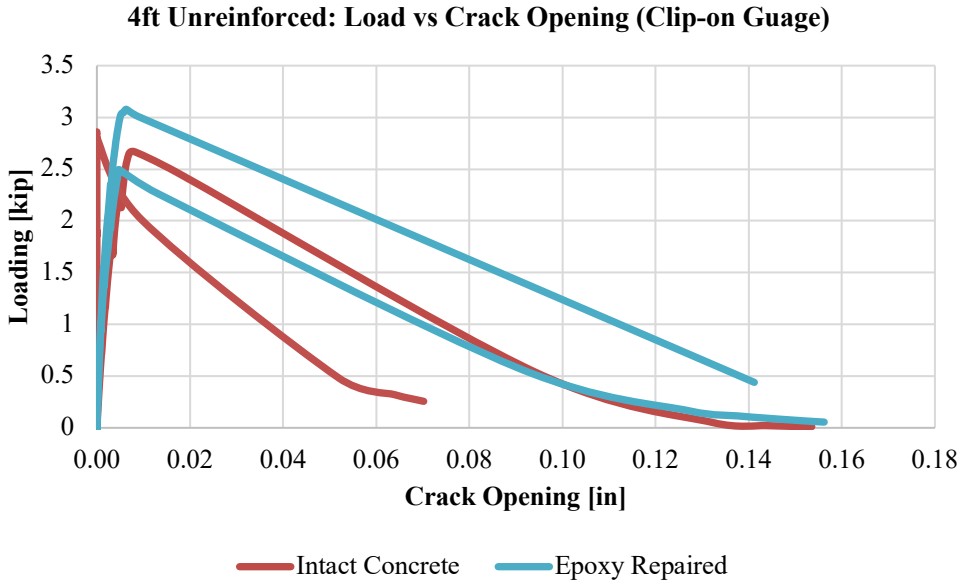

REFERENCES

Ahmad, S., Elahi, A., Barbhuiya, S., and Farooqi, Y. 2013. "Repair of cracks in simply supported beams using epoxy injection technique." *Materials and Structures/Materiaux et Constructions*, 46:1547–1559. doi:10.1617/s11527-012-9996-x.

Akçaoğlu, T. 2017. "Determining aggregate size & shape effect on concrete microcracking under compression by means of a degree of reversibility method." *Construction and Building Materials*, 143:376–386. doi:10.1016/j.conbuildmat.2017.03.128.

Alexander, M., and Mindess, S. 2005. *Aggregates in Concrete*. Taylor & Francis e-Library.

ASTM C1583. 2013. "Tensile Strength of Concrete Surfaces and the Bond Strength or Tensile Strength of Concrete Repair and Overlay Materials by Direct Tension (Pull-off Method)1." *ASTM International*. doi:10.1520/C1583.

ASTM C39. 2016. "Standard Test Method for Compressive Strength of Cylindrical Concrete Specimens." *ASTM International*, 1–7. doi:10.1520/C0039.

ASTM C496. 2017. "ASTM C496-17 Standard Test Method for Splitting Tensile Strength of Cylindrical Concrete Specimens." *Annual Book of ASTM Standards*, 1–5. doi:10.1520/C0496.

Bardella, L. 2001. "A phenomenological constitutive law for the nonlinear viscoelastic behavior of epoxy resins in the glassy state." *Construction and Building Materials*,

21:157–163.

Bazant, Z. P. 1992. “FRACTURE MECHANICS OF CONCRETE · STRUCTURES Part , I State-of-Art Report,” 140:17–30.

Bertero, V. V., Rea, D., Mahin, S., and Atalay, M. B. 1973. “Rate of Loading Effects on Uncracked and Repaired Reinforced Concrete Members.” *Proceedings of 5th World Conference on Earthquake Engineering*, 6:271–278.

Coronado, C. A., and Lopez, M. M. 2008. “Experimental Characterization of Concrete-Epoxy Interfaces.” *Journal of Materials in Civil Engineering*, 20:303–312. doi:10.1177/0892705706055447.

Courard, L., Piotrowski, T., and Garbacz, A. 2014. “Near-to-surface properties affecting bond strength in concrete repair.” *Cement and Concrete Composites*, 46:73–80. doi:10.1016/j.cemconcomp.2013.11.005.

Gamble, W. L. 1997. “Reader Comments: Release methodology of strands to reduce end cracking in pretensioned concrete girders.” *PCI Journal*, 42:102–108. doi:10.15554/pcij.01011997.42.54.

GDOT, Floyd, J., Golden, K., and McMurry, R. 2013. *Standard Specifications Construction of Transportation Systems: Georgia Department of Transportation*.

Gergely, P., and Sozen, M. A. 1967. “Design of Anchorage-Zone Reinforcement in Prestressed Concrete Beams.” *PCI Journal*, 12:63–75.

Griffith, A. A. 1920. “The Phenomena of rupture and flow in solids.” *Phil. Trans. Roy. Soc. London*, C:163–198.

Guo, J. S., and Waldron, P. 2001. “An Elastic Model to Quantify the Effect of Moisture on the Mechanical Properties of Concrete at the Time of Test.” *Magazine of Concrete Research*, 53:151–162.

Hillerborg, A. 1985. “The theoretical basis of a method to determine the fracture energy GF of concrete.” *Materials and Structures*, 18:291–296. doi:10.1007/BF02472919.

Hillerborg, A., Modéer, M., and Petersson, P. E. 1976. “Analysis of crack formation and crack growth in concrete by means of fracture mechanics and finite elements.” *Cement and Concrete Research*, 6:773–781. doi:10.1016/0008-8846(76)90007-7.

Issa, C. A., and Debs, P. 2007. “Experimental study of epoxy repairing of cracks in concrete.” *Construction and Building Materials*, 21:157–163. doi:10.1016/j.conbuildmat.2005.06.030.

Ji, K., Gao, N., Arson, C., Wang, P., Tien, R., and Stewart, L. 2019. *Extended Finite Element Method Model on Repaired Concrete - Unpublished*.

Kannel, J., French, C., and Stolarski, H. 1997. “Release methodology of strands to reduce end cracking in pretensioned concrete girders.” *PCI Journal*, 42:42–54. doi:10.15554/pcij.01011997.42.54.

Kaplan, M. F. 1959. “Flexural and Compressive Strength of Concrete as Affected by the Properties of Coarse Aggregates.” *Journal of the American Concrete Institute*, 55:158–165. doi:10.14359/11415.

Keane, B. F. 2009a. “FIELD GUIDE TO CONCRETE REPAIR Crack Repair by Gravity Feed.” *ACI RAP Bulletin 2*, 1–6.

———. 2009b. “FIELD GUIDE TO CONCRETE REPAIR Structural Crack Repair by Epoxy Injection.” *ACI RAP Bulletin 1*, 1–7.

Lee, J., and Lopez, M. M. 2014. “An Experimental Study on Fracture Energy of Plain Concrete.” *International Journal of Concrete Structures and Materials*, 8:129–139. doi:10.1007/s40069-014-0068-1.

Li, G. 2004. *The Effect of Moisture Content on the Tensile Strength Properties of Concrete*. University of Florida.

Linsbauer, H. N., and Tschegg, E. K. 1986. “Fracture energy determination of concrete with cube-shaped specimens.” *Zement Und Beton*.

Löfgren, I. 2004. “The wedge splitting test – a test method for assessment of fracture parameters of FRC?” *Fracture Mechanics of Concrete Structures FRAMCOS-5*, 1155–1162. Retrieved from http://www.framcos.org/FraMCoS-5/Lofgren.Wedge.pdf.

Man, H. K., and van Mier, J. G. M. 2008. “Influence of particle density on 3D size effects in the fracture of (numerical) concrete.” *Mechanics of Materials*, 40:470–486. doi:10.1016/j.mechmat.2007.11.003.

Man, H. K., and van Mier, J. G. M. 2008. “Size effect on strength and fracture energy for numerical concrete with realistic aggregate shapes.” *International Journal of Fracture*, 154:61–72. doi:10.1007/s10704-008-9270-y.

Mehta, P. K., and Monteiro, P. J. M. 2006. *Concrete: Microstructure, Properties, and Materials*, Third Edit. McGraw-Hill.

Myers, J. J., Nanni, A., Jones, M., Stone, D., Candidate, M. S., Gopalaratnam, V., … Candidate, M. S. 2001. “Precast I-Girder Cracking: Causes and Design Details.”

Okada, K., KobayashiI, K., and Miyagawa, T. 1988. “Influence of longitudinal cracking due to reinforcement corrosion on characteristics of reinforced concrete members.” *ACI Structural Journal*, 85.

PCI. 2001. *Bridge Member Repair Guidelines, Precast/Prestressed Concrete Institute (PCI) Northeast Region*.

Rahim, A., Jansen, D., Abo-Shadi, N., and Simek, J. 2010. “Overview of High-Molecular-Weight Methacrylate for Sealing Cracks in Concrete Bridge Decks.” *Transportation Research Record: Journal of the Transportation Research Board*, 2202:77–81. doi:10.3141/2202-10.

Reichard, B. D. 2015. *Uniaxial Tensile Testing Technique To Obtain Softening Response of Ultra-High Performance Concrete Under Confining Pressures*. Georgia Institute of Technology.

Reinhardt, H. W., Rossi, P., and van Mier, J. G. M. 1990. “Joint Investigation of Concrete at High Rates of Loading.” *Materials and Structures*, 23:213–216.

Rocco, C. G., and Elices, M. 2009. “Effect of aggregate shape on the mechanical properties of a simple concrete.” *Engineering Fracture Mechanics*, 76:286–298. doi:10.1016/j.engfracmech.2008.10.010.

Rodler, D. J., Whitney, D. P., Fowler, D. W., and Wheat, D. L. 1989. “Repair of Cracked Concrete with High Molecular Weight Methacrylate Monomers.” *Polymers in*

Concrete: Advances and Applications, 113–127.

Ross, C. A., Jerome, D. M., Tedesco, J. W., and Hughes, M. L. 1996. "Moisture and strain rate effects on concrete strength." *Materials Journal*, 93:293–300.

Sadowski, Czarnecki, S., and Hoła, J. 2016. "Evaluation of the height 3D roughness parameters of concrete substrate and the adhesion to epoxy resin." *International Journal of Adhesion and Adhesives*, 67:3–13. doi:10.1016/j.ijadhadh.2015.12.019.

Schlangen, E., and van Mier, J. G. M. 1992a. "Experimental and numerical analyses of micromechanisms of fracture of cement-based composites." *Cement and Concrete Composites*, 14.

———. 1992b. "Simple lattice model for numeri- cal simulations of fracture of concrete materials and structures." *Materials and Structures*, 25.

Shin, H. C., Miyauchi, H., and Tanaka, K. 2011. "An experimental study of fatigue resistance in epoxy injection for cracked mortar and concrete considering the temperature effect." *Construction and Building Materials*, 25:1316–1324.

Tadros, M. K., Badie, S. S., and Tuan, C. Y. 2010. *NCHRP Report 654*. National Cooperative Highway Research Program. doi:10.17226/13746.

Transpo Industries. 2017a. "Sealate T-70 Product Sheet."

———. 2017b. "Sealate T-70 Technical Data Sheet."

van Mier, J. G. M. 2012. *Concrete Fracture*. doi:10.1201/b12968.

Wang, P., Tien, R., Arson, C., Ji, K., Gao, N., and Stewart, L. 2019. *Discrete Element*

Method Model on Repaired Concrete - Unpublished.

Xu, H., and Arson, C. 2014. "Anisotropic damage models for geomaterials: theoretical and numerical challenges." *International Journal of Computational Methods*, 11.

Xu, H., Busetti, S., and Arson, C. 2017. "Fracture-induced anisotropy of the stress–strain response of shale at multiple scales." *International Journal of Geomechanics*, 17.